Insulin secretion deficits in a Prader-Willi syndrome β-cell model are associated with a concerted downregulation of multiple endoplasmic reticulum chaperones

Erik A. Koppes[1], Marie A. Johnson[1], James J. Moresco[2,#], Patrizia Luppi[3], Dale W. Lewis[4], Donna B. Stolz[3], Jolene K. Diedrich[2], John R. Yates III[2], Ronald C. Wek[5], Simon C. Watkins[3], Susanne M. Gollin[4], Hyun J. Park[4], Peter Drain[3], Robert D. Nicholls[1]

[1] Division of Genetic and Genomic Medicine, Department of Pediatrics, UPMC Children's Hospital of Pittsburgh, Pittsburgh, PA 15224; [2] Department of Molecular Medicine and Neurobiology, The Scripps Research Institute, La Jolla, CA 92037; [3] Department of Cell Biology, University of Pittsburgh School of Medicine, Pittsburgh, PA 15261; [4] Department of Human Genetics, University of Pittsburgh School of Public Health, Pittsburgh, PA 15261; [5] Department of Biochemistry and Molecular Biology, Indiana University School of Medicine, Indianapolis, IN 46202

Address correspondence to R.D.N.:
Dr. Robert D. Nicholls, Department of Pediatrics, UPMC Children's Hospital of Pittsburgh, Rangos Research Building, 4401 Penn Avenue, Pittsburgh, PA 15224; robert.nicholls@chp.edu; Tel., 1-412-692-7855; Fax, 1-412-692-7816.

[#] Current address: Center for Genetics of Host Defense, UT Southwestern Medical Center, Dallas, TX

Keywords: CRISPR/Cas9; genomic imprinting; hormone secretion; metabolic disease; pancreatic islet

ABSTRACT

Prader-Willi syndrome (PWS) is a multisystem disorder with neurobehavioral, metabolic, and hormonal phenotypes, caused by loss of expression of an imprinted gene cluster. Prior evidence from a PWS mouse model identified abnormal pancreatic islet development with deficient insulin secretion. To investigate PWS-genes in β-cell function, we used genome-editing to generate isogenic, clonal INS-1 insulinoma lines having deletions of the silent, maternal (control) or active, paternal PWS-alleles. PWS β-cells demonstrated a cell-autonomous reduction in insulin secretion. Further, proteomic analyses revealed reduced levels of cellular and secreted insulin peptides concomitant with reduction of numerous endoplasmic reticulum (ER) chaperones, including GRP78 and GRP94. Critically, transcriptomic studies demonstrated that only the ER chaperone deficit originated from transcriptional downregulation. Thus, a chronic widespread deficit of ER chaperones in PWS β-cells, similar to reports of acute ablation of single ER chaperones but precluding dosage compensation, is hypothesized to lead to a delay in folding and/or ER transit of insulin and other secretory pathway cargo. These findings implicate PWS-imprinted genes in concerted regulation of ER chaperone biosynthesis and β-cell secretory pathway function, illuminating the pathophysiological basis of hormone deficits in PWS.

46 **INTRODUCTION**

47 Prader-Willi syndrome (PWS) is a multisystem disorder caused by loss of
48 expression of a large contiguous cluster of paternally-expressed, imprinted genes from
49 human chromosome 15q11.2 (Chung et al., 2020; Costa et al., 2019; Tauber and Hoybye,
50 2021). Clinically, PWS is characterized by failure to thrive (FTT) with hypotonia,
51 developmental and cognitive delay, behavioral problems, short stature, hypogonadism,
52 hyperphagia, and early-onset obesity (Muscogiuri et al., 2019; Tauber and Hoybye,
53 2021). Prominent endocrine features of PWS include deficiencies of multiple hormones,
54 including growth hormone (GH), oxytocin, gonadotropins, insulin-like growth factor (IGF-
55 I), thyroid hormones, amylin (IAPP), and pancreatic polypeptide (PP) (Costa et al., 2019;
56 Deal et al., 2013; Fountain and Schaaf, 2015; Hirsch et al., 2015; Lee et al., 2011;
57 Muscogiuri et al., 2019; Tomita et al., 1989). In addition, plasma insulin is lower than
58 expected in PWS relative to the degree of obesity (Goldstone et al., 2005; Paik et al.,
59 2007; Schuster et al., 1996). Episodes of hypoglycemia have been reported in PWS
60 patients, suggesting an imbalance in glucose homeostasis (Harrington et al., 2014; Ma et
61 al., 2012). In contrast, plasma ghrelin is grossly elevated in PWS (Cummings et al., 2002;
62 Goldstone et al., 2005; Tauber and Hoybye, 2021). Although the PWS literature suggests
63 a hypothalamic etiology (Tauber and Hoybye, 2021), the mechanisms for endocrine and
64 metabolic dysfunction in PWS have not been elucidated.

65 The PWS-imprinted domain is comprised of ten paternally-expressed imprinted
66 genes conserved in human and rodents (with an additional two genes each unique to
67 human and rodents), encoding lncRNAs, snoRNAs, miRNAs, or distinct proteins (Cavaillé
68 et al., 2000; Chen et al., 2020; Chung et al., 2020; Costa et al., 2019; Gray et al., 1999a;
69 Kishore and Stamm, 2006; Nicholls and Knepper, 2001; Wu et al., 2016). These imprinted

70 genes are predominantly expressed in neuronal (Castle et al., 2010; Cavaillé et al., 2000;
71 Kishore and Stamm, 2006) and neuroendocrine lineages (Chen et al., 2020), as well as
72 pancreatic endocrine cells (α-, β-, δ-, and PP cells, with only low expression in acinar,
73 ductal, or undefined cells) based on recent gene-specific (Stefan et al., 2011) and single
74 cell RNA sequencing (scRNA-seq) studies (Benner et al., 2014; Li et al., 2016a;
75 Segerstolpe et al., 2016). Further, *SNRPN* has decreased islet expression in β-cell failure
76 due to saturated fatty acids (Cnop et al., 2014) or cytokines (Eizirik et al., 2012), while
77 *SNORD116* and *SNORD107* occur in islet exosomes and decrease by IL-1β and IFN-γ
78 treatment (Krishnan et al., 2019). Finally, *SNORD116* RNA levels are greatly reduced in
79 MODY3 β-cells (Low et al., 2021). These observations suggest that PWS-gene products
80 function in the endocrine pancreas including in β-cells.

81 Our earlier studies of a transgenic-PWS (TgPWS) mouse model harboring a
82 deletion of the orthologous PWS-imprinted domain demonstrated severe FTT,
83 abnormalities in fetal pancreatic islet development and architecture, reduced α- and β-
84 cell mass, increased apoptosis, and postnatal onset of progressive hypoglycemia that led
85 to lethality within the first postnatal week (Stefan et al., 2005; Stefan et al., 2011). Plasma
86 insulin and glucagon levels were low during fetal and neonatal life of TgPWS mice (Stefan
87 et al., 2005; Stefan et al., 2011), and, at postnatal day 1 (P1) prior to onset of
88 hypoglycemia, there was significantly reduced basal and glucose-stimulated insulin
89 secretion (GSIS) from cultured TgPWS islets (Stefan et al., 2011). Furthermore, using an
90 insulin-Timer fluorescent protein biomarker to image P1 β-cells *in vivo*, TgPWS mice
91 showed a striking accumulation of aged insulin whereas wildtype control littermates only
92 displayed newly synthesized insulin (Stefan et al., 2011). These results suggested that

93 PWS-imprinted genes are required for the development and secretory function of
94 pancreatic endocrine cells.

95 Based on the salient insulin secretion dysfunction in the PWS-mouse model
96 (Stefan et al., 2011), we sought to assess the role of PWS genes in pancreatic β-cell
97 secretory pathway function in a cellular model system. Herein, we used CRISPR/Cas9
98 genome editing within the INS-1(832/13) insulinoma (β)-cell line (Hohmeier et al., 2000)
99 to generate deletions of the complete PWS-domain. Following validation of a cell-
100 autonomous insulin secretion deficit in the PWS INS-1 model, we performed molecular
101 profiling by proteomic and transcriptomic approaches. The data revealed deficits in
102 multiple secreted hormones as well as endoplasmic reticulum (ER) chaperones that are
103 components of secretory protein folding and trafficking pathways (Kalwat et al., 2021;
104 Rajpal et al., 2012; Sharma et al., 2021; Sun et al., 2019; Yong et al., 2021; Zhu and Lee,
105 2015), providing mechanistic insight into PWS-gene function in pancreatic β-cells.

106 **RESULTS**

107

108 ***Generation of INS-1 cell lines with PWS-gene deletions:*** Various insulinoma cell lines,
109 predominantly of rodent origin, are widely utilized to investigate β-cell mechanisms as a
110 tractable *in vitro* model system (Skelin et al., 2010). To investigate the functions of PWS-
111 genes in β-cells, we used CRISPR/Cas9 genome-editing to target 3.16 Mb deletions
112 encompassing the PWS-genes (**Fig. 1A**; **Fig. S1A**) in rat INS-1(832/13)::mCherry
113 insulinoma cells (hereafter termed INS-1) that secrete rat and human insulin (Hohmeier
114 et al., 2000) and express a mouse *Ins2* C-peptide-mCherry biosensor in insulin secretory
115 granules (Watkins et al., 2002). The large deletions were visualized in about 9% of
116 unselected, transfected cells as determined by fluorescence *in situ* hybridization (FISH)
117 (**Fig. S1B**). INS-1 lines with PWS-domain deletions were derived through sequential
118 targeting and clonal isolation of cell lines initially harboring deletions of the silent maternal
119 allele, followed by targeting of the remaining paternal loci, culminating in the creation of
120 homozygous PWS-deletion lines (**Fig. 1B**). This process first led to isolation of two lines
121 with a PWS-region deletion (5-5, 5-9) identified by deletion-breakpoint PCR (**Fig. 1C**) and
122 DNA sequencing (**Fig. S2A,B**), and confirmed by FISH using BAC probes from within and
123 outside the PWS-domain (**Fig. S1C-F**). One PWS allele was deleted in all interphase and
124 metaphase cells of line 5-5 (**Fig. S1D**), indicating clonal isolation of a cell line with a PWS-
125 domain deletion. Initially, line 5-9 was more complex, as FISH showed two cell types with
126 either no deletion (most cells) or a PWS-domain deletion (**Fig. S1E**); additionally, similar
127 proportions of cells lacked mCherry fluorescence, likely due to epigenetic silencing (as
128 DNA analysis indicated the transgene was present) or were mCherry-positive,
129 respectively. This allowed separation by fluorescence-activated cell sorting (FACS), with

130 establishment of a clonal mCherry-positive cell line (5-9) harboring a PWS-domain
131 deletion (**Fig. S1F**). Clonal engineered cell lines 5-5 and 5-9 were inferred to have
132 maternal-deletions of the rat PWS-domain as evidenced by **1)** detection of only an
133 unmethylated allele at the PWS-imprinting center (PWS-IC) by bisulfite PCR whereas
134 parental INS-1 and control lines had biparental DNA methylation (**Fig. 1D**); and **2)**
135 expression of PWS-imprinted loci by reverse-transcription-PCR (RT-PCR) (**Fig. S1G**),
136 indicating the presence of an active, paternal-allele (**Fig. S1H**). Finally, the presence of
137 mutations at sgRNA target sites on the intact, paternal chromosome, termed scarred
138 mutation alleles, identified a single nucleotide insertion at the sgRNA1 site (**Fig. S1I**; **Fig.**
139 **S2C-E**) but different nucleotide insertions at the sgRNA3 site (**Fig. S1I**; **Fig. S2F-H**), the
140 latter indicating an independent origin for the cell lines, 5-5 and 5-9. In contrast, no
141 sequence changes occurred at top-ranked off-target sites for sgRNA1 or sgRNA3 (**Fig.**
142 **S3**).

143 To specifically target the paternal allele of lines 5-5 and 5-9, we used rat-specific
144 sgRNA sets internal to the first targeting sites to generate slightly smaller 3.143 Mb PWS-
145 deletions (**Fig. S4A-C**). The use of FISH demonstrated that about 5% of unselected,
146 transfected cells had a PWS-deletion (**Fig. S4D**). We chose maternal deletion (control)
147 line 5-9 for a second round of transfections and clonal isolation, generating control lines
148 2 and 16 (**Fig. 1B,E**; **Fig. S4E,F**) as well as PWS lines 19 and 25, with an expected
149 paternal deletion-PCR product and PWS line 3 with a larger than expected deletion-PCR
150 product (**Fig. 1B,E**; **Fig. S4G**). DNA sequencing confirmed PWS-deletion breakpoints for
151 lines 19 and 25 (**Fig. S5A-C**) as well as for line 3, although the latter arose from a larger
152 deletion at an alternate (alt) proximal alt-sgRNA70-3 targeting site with a DNA repair event
153 that inserted a fragment of *E. coli* DNA in the breakpoint junction (**Fig. S5D**). FISH studies

154 confirmed that lines 3 and 25 had deletions of the PWS-domain on each allele (**Fig.**
155 **S4H,I**); however, FISH analysis also revealed that line 25 was mosaic for cells with diploid
156 or tetraploid PWS-signals (**Fig. S4I**). Consequently, line 25 was not used further. In
157 contrast, line 19 had a residual fraction of cells (1-3.7%) with an intact paternal allele as
158 shown by FISH (**Fig. S4J**) and droplet digital PCR (ddPCR) (**Fig. S6**) which was removed
159 by cell dilution and isolation of five clonal lines 19-1 through 19-5 (**Fig. 1B**; **Fig. S4K,L**;
160 **Fig. S10A**). Finally, sgRNA target sites not deleted or involved in a deletion breakpoint
161 were assessed for scarred mutation alleles identifying a 28-nt deletion at alt-sgRNA70-3
162 in PWS lines 19-1 and 19-4 (**Fig. S4N**; **Fig. S5E-L**), while no sequence changes occurred
163 at top-ranked off-target sites for sgRNA70-3 (**Fig. S7**) or sgRNA79-1 (**Fig. S8**).

164 Genomic copy number was confirmed by ddPCR (**Fig. 1F**; **Fig. S6**; **Fig. S9**),
165 establishing a set of three control lines (5-9, 2, 16) with hemizygosity for maternal-allele
166 deletions (**Fig. S1H**) and three PWS INS-1 lines (3, 19-1, 19-4) with homozygosity for
167 PWS-domain deletions (**Fig. S4M**). An absence of PWS-gene expression in all PWS lines
168 was shown by RT-PCR for each PWS-imprinted gene (**Fig. 1G**; **Fig. S10A,B**) and by
169 western blot analysis for the SmN polypeptide encoded by *Snrpn* (**Fig. 1H**). Intriguingly,
170 PWS INS-1 lines showed a very low level of apparent expression of the PWS-imprinted
171 gene *Snurf* by RT-PCR (**Fig. S10A**; **Fig. S11A,B**). Sequencing of the RT-PCR products
172 identified an expressed *ψSnurf* sequence within a recently evolved *ψSnurf-ψSnrpn* locus
173 located in an intron of the *Mon2* gene (**Fig. S11B,C**). Using a *Pml*I variant between *Snurf*
174 and *ψSnurf* (**Fig. S11D**), we confirmed expression specifically of *ψSnurf* with complete
175 silencing of *Snurf* (**Fig. S11B**), as expected for PWS INS-1 lines. Scattered mutations in
176 the *ψSnurf* (**Fig. S11D**) and *ψSnrpn* (**Fig. S11E,F**) segments likely inactivate any coding

177 potential (**Fig. S11G, H**). In summation, these results establish a panel of clonal INS-1
178 lines homozygous for ~ 3.16 Mb deletions, also termed PWS β-cell lines, and similarly, of
179 clonal control lines with a deletion only involving the silent, maternal allele.
180
181 ***PWS INS-1 cell lines show deficits in insulin secretion and ER chaperones:*** To
182 determine whether PWS INS-1 cell lines have secretory deficits, we carried out insulin
183 secretion assays under low (2.2 mM) and high (22 mM) glucose conditions. The three
184 PWS cell lines displayed a striking deficit in both basal and glucose-induced insulin
185 secretion as compared to the isogenic control INS-1 lines (**Fig. 2**). However, both the
186 PWS and control cell lines had a similar increase from each basal level for GSIS (**Fig. 2**),
187 indicating that PWS β-cells were not deficient in glucose responsiveness.
188 Next, mass spectrometry was used to assess changes in the cellular proteome
189 and all secreted peptides in PWS *vs.* control INS-1 cell lines, under insulin secretion
190 conditions of 22 mM glucose, separating cellular proteins by methanol-acetic acid
191 extraction into soluble (mostly small) and insoluble (mostly large) protein fractions with
192 the latter analyzed by quantitative proteomics (**Fig. 3A**). Unexpectedly, in PWS INS-1
193 cells there was a striking deficiency of multiple ER chaperone proteins, including
194 GRP78/BiP (HSPA5), GRP94/endoplasmin (HSP90B1), PDIA4, HYOU1, CRELD2, and
195 DNAJB11, with lesser reductions in SDF2L1, DNAJC3, PDIA6, and PDIA3, and a modest
196 decrease in PPIB (**Fig. 3B**). Similar deficits of residual amounts of many of these ER
197 chaperones as well as MANF were detected in the soluble protein fraction (**Fig. 3C**).
198 Furthermore, in PWS β-cell lines there was reduced abundance of numerous hormones
199 co-secreted from INS-1 cells, including rat insulin-1 and insulin-2, mouse insulin-2, and
200 human insulin (pre-pro-, pro-, C-peptide, and mature versions of each), as well as

201 reductions in processed and precursor forms of IAPP and NPY, detected in both the
202 cellular small protein fraction (**Fig. 3C**) and residual amounts in the large protein fraction
203 by quantitative proteomics (**Fig. 3B**). In contrast, the full-length secretory granule protein,
204 chromogranin B (CHGB), and the C-terminal CHGB (CCB)-peptide were increased 2-fold
205 (**Fig. 3B,C**). Extending both the insulin secretion data (**Fig. 2**) and the cellular protein
206 deficiencies (**Fig. 3B,C**), mass spectrometry analysis of peptides secreted into the culture
207 media demonstrated reduced levels of all forms of insulins and IAPP in PWS β-cell media
208 compared to control (**Fig. 3D**). There was also a reduction in secreted levels of the 14
209 amino acid WE14 peptide processed from chromogranin A (CHGA), but no changes in
210 the CHGA precursor and processed forms in either secreted or cellular fractions.
211 Secreted levels of chromogranin B were increased in PWS (**Fig. 3D**), further illustrating
212 the concordance between cellular and secreted peptide levels in PWS *vs.* control INS-1
213 lines. These results indicate that deletion of PWS-genes sharply lowers secretion of
214 insulin and other peptide hormones (IAPP, NPY, CHGA-WE14) and this reduction is
215 associated with deficiencies in many ER chaperones.

216

217 ***Reduced mRNA levels for hormones and ER chaperones in PWS INS-1 cell lines:***
218 Many of the PWS-imprinted genes (**Fig. 1A**) are suggested to function in gene expression
219 (Cavaillé et al., 2000; Gray et al., 1999a; Gray et al., 1999b; Kishore and Stamm, 2006;
220 Liu et al., 2014; Wu et al., 2016). To gain insight into the molecular basis for insulin
221 secretion and ER chaperone deficits in PWS INS-1 lines, high-throughput total RNA
222 sequencing (RNA-seq) was used to identify differentially expressed genes (DEGs) (**Fig.
223 4A-C**; **Tables S1,S2**). Visualization by a heatmap clustergram (**Fig. 4A**) indicates that

224 PWS clonal lines and control clonal lines each grouped together with similar expression
225 profiles. A volcano plot depicting the magnitude, direction, and statistical significance of
226 DEGs in the 3 PWS *vs.* 3 control lines illustrates no appreciable expression (Log2 Fold
227 Change < -5) of PWS-imprinted genes with remaining DEGs symmetrically orientated
228 around the ordinate axis with a near equivalent number of significantly upregulated (105)
229 and downregulated (123) genes (**Fig. 4B**). The PWS transcripts with complete loss of
230 expression specifically in PWS INS-1 lines include *Snurf*, *Snrpn*, *Ipw*, *Mkrn3*, all four
231 snoRNAs (*Snord116, Snord115, Snord107* and Snord*109*), miRNA (*Mir344* isoforms),
232 and duplicated U1-*Snurf* sequences (**Fig. 4B**), as also seen by RT-PCR (**Fig. 1G**; **Fig.**
233 **S10A,B**; **Fig. S11A,B**). Three PWS-imprinted genes, *Ndn*, *Magel2*, and *Frat3* (*Peg12*),
234 were not detected as DEGs as these are not expressed by RT-PCR or RNA-sequencing
235 in any of parental, control, or PWS INS-1 lines. These loci are present by genomic PCR,
236 suggesting an epigenetic inactivation in the INS-1 founder cell line, although silencing is
237 not widespread, as *Mkrn3* and *Mir-344* are interspersed with the silenced loci (see **Fig.**
238 **1A**) and are well-expressed in control INS-1 lines (**Fig. S10B**; **Fig. S12**).

239 To ensure complete coverage of the INS-1 transcriptome, RNA-seq of small stable
240 RNAs in the PWS *vs.* control cell lines was carried out, culminating in the identification of
241 58 significant differentially expressed miRNAs and snoRNAs (**Fig. S12A,B**; **Table S3**).
242 Congruent with the RNA-seq data, all but three correspond to PWS-imprinted small
243 RNAs, including duplicated *MiR-344*, *Snord116* and *Snord115* loci, as well as single copy
244 *Snord107* and *Snord64* loci (**Fig. S12A,B**). In addition, *Mir135b*, *Mir3065*, and *Mir212*
245 were downregulated in PWS INS-1 lines (**Fig. S12B**), although predicted targets were not
246 DEGs by RNA-seq. Eleven of the top 25 highly expressed miRNAs in the rat INS-1 β-cell

247 model (**Table S4**), including *Mir375*, *Mir148a*, *Mir183*, *Mir30d*, *Mir27b*, *Mir25*, *Mir26a2*,
248 *Mir26a*, *Mir192*, *Mir125a*, and *Mir141* are also in the top 25 expressed miRNAs for a
249 human β-cell model (Lawlor et al., 2019). Within INS-1 cells, expression of PWS-region
250 *Snord116* copies make up 13.8% of the top 188 highly expressed snoRNAs and
251 cumulatively would be the thirteenth highest expressed, with *Snord64* also in and
252 *Snord107* just outside the top 100 (**Table S5**), although snoRNAs are poorly studied as
253 a small RNA class.

254 In addition to the loss of PWS-imprinted gene expression in the PWS INS-1 lines,
255 four additional classes of DEGs were identified by manual annotation analysis of RNA-
256 seq data (**Fig. 4B**). These DEG classes encoded: **1)** hormones (e.g., *Iapp*, *Npy*,
257 *mIns2::mCherry*) that were significantly reduced; **2)** nine ER chaperones that were
258 lowered including *Sdf2l1*, *Hspa5*, *Creld2*, *Dnajb11*, *Hyou1*, *Pdia4*, *Dnajc2*, *Hsp90b1*, and
259 *Pdia6*; **3)** "neuronal active zone" proteins that had increased expression, including
260 *Cacna1a*, *Rph3al*, *Bsn*, *Rimbp2*, *Cacna1d*, *Pclo*, and *Chgb*, many of which also play a
261 role in insulin exocytosis (Fan et al., 2017; Fujimoto et al., 2002; Matsunaga et al., 2017;
262 Obermuller et al., 2010; Proverbio et al., 2013; Reinbothe et al., 2013); and **4)** two related
263 transmembrane proteins involved in vesicle acidification (*Tmem176a,b*) (Drujont et al.,
264 2016) whose expression were also enhanced. Gene ontology and pathway analysis of
265 downregulated genes (excluding PWS-imprinted genes) through Enrichr or DAVID
266 highlighted enrichment of multiple ER functional groups including those in ER protein
267 processing, and the unfolded protein response (UPR) that are linked with both IRE1 and
268 ATF6 (**Fig. 4C**; **Fig. S13A-C**). Finally, based on the input of downregulated DEGs, Enrichr
269 predicted potential upstream transcriptional regulatory factors, including NFYA/NFYB (a

270 cofactor of ATF6α, hereafter ATF6), CPEB1, RFX5, IRF3, CREB1, SREBF1, XBP1, and
271 PPARB/D (**Fig. S14**).

272 Transcriptional changes observed by RNA-seq were corroborated by RT-droplet
273 digital PCR (RT-ddPCR) analyses using RNA from independent biological replicates of
274 each PWS and control INS-1 line (**Fig. 4D-H**; **Fig. S15**; **Fig. S16**). We validated equal
275 expression of the housekeeping gene, *Gapdh*, and loss of expression of *Snord116* (**Fig.**
276 **4D**), as well as significant down-regulation in PWS INS-1 lines of 10 genes encoding ER
277 chaperones (**Fig. 4E**: *Hspa5*, *Hsp90b1*, *Pdia4*, *Pdia6*, *Ppib*, *Creld2*, *Sdf2l1*, *Dnajb11*,
278 *Dnajc3*, and *Hyou1*), of endogenous hormones (**Fig. 4F**: *Npy*, *Iapp*), and of the mouse
279 *Ins2-mCherry* transgene (**Fig. 4G**). Further, another eight downregulated genes in PWS
280 β-cells were verified (**Fig. S16**) including *Syt1*, encoding a Ca^{2+}-sensor (Nakajima-Nagata
281 et al., 2004) and *Jph3*, encoding a junctophilin involved in ER-plasma membrane contact
282 bridges (Li et al., 2016b); each with roles in insulin secretion (Li et al., 2016b; Nakajima-
283 Nagata et al., 2004); *Derl3*, involved in ER-associated degradation (ERAD) (Oda et al.,
284 2006), *Mylip*, encoding an E3 ubiquitin ligase regulating the LDL receptor (van Loon et
285 al., 2019), *Atp10a*, encoding a lipid flippase (Naito et al., 2015), and *Tap1* and *Tap2*,
286 encoding ER antigenic peptide transporters that play a role in type 1 diabetes
287 (Kronenberg-Versteeg et al., 2018). Additionally, up-regulation of four genes was
288 confirmed by RT-ddPCR (**Fig. 4H**), including *Cacna1a*, *Chgb*, *Tmem176a*, and
289 *Tmem176b*.

290 Several other observations merit note. In contrast to the proteomics data wherein
291 all endogenous forms of insulin were decreased in PWS INS-1 lines, neither rat *Ins1* nor
292 *Ins2* mRNA levels were statistically different between PWS and control lines in the RNA-
293 seq or RT-ddPCR (**Fig. 4F**) expression profiling. Only a minority of DEGs identified by

294 RNA-seq did not validate by RT-ddPCR, including several encoding neuronal active zone
295 proteins (**Fig. S16**), possibly arising from cell culture media differences between biological
296 replicates. Additionally, an apparent increase in expression of the human *INS-neoR*
297 transgene in PWS lines (**Fig. 4G**) was an artifactual consequence of epigenetic silencing
298 of the transgene, specifically in control line 16 (**Fig. S15A,I-K,M**). Interestingly, although
299 both mRNA (*Pcsk1*) and protein levels of prohormone convertase PC1 were reduced in
300 iPSC-derived neurons from PWS patients and in whole islets of inbred *Snord116*-deficient
301 mice (Burnett et al., 2017; Chen et al., 2020), neither PC1 protein nor *Pcsk1* mRNA levels
302 were changed in PWS INS-1 cell lines (**Fig. 4F**). Finally, no markers of activation of
303 apoptotic or other cell death pathways were observed by RNA-seq or proteomics,
304 consistent with the absence of any increase in cell death observed in cultured PWS or
305 control INS-1 cells. Indeed, electron microscopy showed normal mitochondria, rough ER,
306 and other subcellular organelles in PWS and control INS-1 lines (**Fig. S17**). The
307 difference in observations *in vivo* where increased apoptosis was observed in a subset of
308 α- and β-cells in TgPWS fetal islets (Stefan et al., 2011) and *in vitro* (this study) may
309 reflect the use of enriched culture medium with reduced cellular stress under cell culture
310 conditions. In summary, the transcriptome studies show that loss of PWS-gene
311 expression in PWS β-cell lines is accompanied by widespread alterations in mRNA levels
312 most notably encoding secreted peptides and ER chaperones.
313
314 ***Confirmation of insulin and ER chaperone protein deficits in PWS INS-1 lines:*** To
315 further address the predicted disruptions of the ER and secretory pathway, we used
316 western blot analyses to measure cellular levels of insulin and ER chaperones in control
317 and PWS INS-1 lines. Levels of numerous forms of insulin polypeptides detected by an

318 anti-insulin antibody were each significantly decreased in PWS INS-1 lines compared to
319 controls, including diminished amounts of pro-insulin, pre-pro-insulin, and pro-mInsulin-
320 2::mCherry bands (**Fig. 5A,D**). Additionally, using an anti-mCherry antibody, we observed
321 that PWS cells have significantly lower levels of the proinsulin form of the mouse insulin2-
322 mCherry transgene but no decrease in the processed C-peptide (CP) form (**Fig. 5B,E**).
323 Indeed, confocal microscopy of the processed CP-mCherry shows punctate cytoplasmic
324 compartmentalization without a discernable difference between PWS and control INS-1
325 lines (**Fig. S18**). Importantly, use of a KDEL antibody to identify proteins with the ER
326 retention motif confirmed significant deficiencies in levels of the two major ER chaperone
327 proteins, GRP78/BiP and GRP94, in PWS INS-1 cell lines (**Fig. 5C,F**). These results
328 indicate that there are major disruptions of the protein folding machinery and attendant
329 reductions in insulin processing and secretion in the PWS INS-1 cells.
330
331 ***PWS INS-1 cells are more sensitive to activation by ER stressors:*** Chaperones, such
332 as GRP78 and GRP94, not only have essential roles in protein folding and trafficking in
333 the ER but disruptions of chaperone functions sensitize cells to agents that stress this
334 organelle (Bertolotti et al., 2000; Braakman and Bulleid, 2011; Hong et al., 2004; Shen et
335 al., 2002; Teske et al., 2011; Tsuchiya et al., 2018). Therefore, we assessed whether the
336 PWS INS-1 lines and their reduced levels of ER chaperones (**Fig. 3-5**) would accentuate
337 activation of the three sensory proteins of the UPR. First, ER stress activates IRE1α to
338 catalyze mRNA processing of the *Xbp1* mRNA to generate the functional XBP1
339 transcription factor (Tsuchiya et al., 2018); this non-canonical "splicing" of *Xbp1*
340 transcripts occurs at low and equal levels in PWS and control INS-1 cells under DMSO
341 control growth conditions but is enhanced by treatment with thapsigargin to initiate ER

342 stress (**Fig. 6A,D**; **Fig. S19A,B**). Importantly, production of "spliced" *Xbp1* mRNA in
343 thapsigargin-treated cells occurs significantly more robustly at earlier 2 h and 3 h
344 timepoints for PWS than for control INS-1 lines (**Fig. 6A,D**; **Fig. S19A,B**) but normalizes
345 by 4-5 h (**Fig. S19A,B**). These results reveal that while the initial magnitude of IRE1
346 activation is greater in the PWS INS-1 cells, the duration and cumulative response is
347 comparable. Second, phosphorylation of eIF2α by PERK (Teske et al., 2011) was
348 assessed, with PWS INS-1 lines showing significantly higher levels of eIF2α pSer51
349 phosphorylation than control lines when ER stress was induced by 5 h of thapsigargin
350 treatment (**Fig. 6B,E**). Phosphorylated eIF2α inhibits general translation but preferentially
351 translates certain stress adaptive genes, including ATF4 and CHOP; transcripts of these
352 genes were unaffected in unstressed PWS INS-1 cells as measured by RNA-seq.

353 Third, dissociation of ER-retained ATF6 from GRP78 by ER stressors such as de-
354 glycosylation agents (Hong et al., 2004; Shen et al., 2002) enable it to move to the Golgi,
355 where it is processed to an activated nuclear (N) form, ATF6-N, which regulates
356 expression of genes encoding many ER chaperones, including GRP78 and others. In
357 PWS and control INS-1 cells, ER stress induced by tunicamycin, as expected, de-
358 glycosylates full-length glycosylated (FL-G) ATF6 of ~ 102-kD to an unglycosylated 90-
359 kD (FL-UG) form and the processed ATF6-N form of 55-kD (**Fig. 6C**; **Fig. S20A**). The
360 loss of the ATF6 FL-G form by deglycosylation occurs at the same rate for PWS and
361 control cell lines (**Fig. S20B**). However, the ratio of the processed ATF6-N (due to higher
362 production in PWS than control INS-1 cells) to full-length unglycosylated 90-kD (with a
363 higher level in control than PWS INS-1 cells) is significantly greater for PWS compared
364 to control INS-1 cells at 2-5 h timepoints (**Fig. 6C,F**; also see **Fig. S20A,B**). Thus, ATF6
365 is being activated to ATF6-N earlier and more robustly in PWS than in control INS-1 β-

366 cell lines. Combined, these results on ER stress activation of the IRE1α/XBP1,
367 PERK/eIF2α, and ATF6-N pathways indicate that PWS INS-1 β-cells are more sensitive
368 than control INS-1 β-cells to ER stressors.

369 **DISCUSSION**

370 Although PWS has long been assumed to be a neuroendocrine disease of the
371 hypothalamus (Chen et al., 2020; Tauber and Hoybye, 2021), studies using mouse
372 models have implicated a role for the pancreatic endocrine system (Burnett et al., 2017;
373 Stefan et al., 2011). Here, we generated a novel INS-1 β-cell model through deletion of
374 the ~ 3.16 Mb PWS-orthologous imprinted domain in which to investigate PWS β-cell
375 biology. The PWS deletion results in a β-cell autonomous defect in both basal and
376 regulated insulin secretion, although the latter is at least in part consequent to the effect
377 on basal insulin secretion. The PWS deletion also results in cell autonomous deficits in
378 the secretion of other peptide hormones and in deficiencies of β-cell ER chaperones
379 required for folding, exit and trafficking of secretory peptides. Presciently, studies reported
380 25 years ago demonstrated that PWS adults compared to matched obese controls had
381 significantly reduced first- and second-phase insulin secretion during intravenous glucose
382 tolerance tests (Schuster *et al.*, 1996), attesting to the translational relevance of the PWS
383 INS-1 model. These findings strongly support a hypothesis that PWS-genes are required
384 for fundamental β-cell mechanisms affecting production of peptide hormones.

385 Basal insulin secretion and GSIS are dramatically reduced both *in vivo* in the
386 TgPWS-deletion mouse model (Stefan et al., 2011) and the new *in vitro* PWS INS-1 β-
387 cell model. As PWS β-cells in both models are glucose-responsive this indicates the
388 defect is in a fundamental component of the secretory apparatus. In TgPWS mice,
389 perinatal pancreatic insulin secretion dysfunction was associated with intracellular
390 retention of aged insulin and reduced islet insulin and C-peptide content as well as
391 reduced islet glucagon content and plasma glucagon levels suggestive of broader

392 endocrine cell dysfunction (Stefan et al., 2011). Similarly, in our current study we have
393 found that all insulin isoforms that are expressed in and secreted from the PWS INS-1 β-
394 cell are decreased, as measured by proteomics and western blot analyses. Remarkably,
395 these equivalent insulin secretion deficits between PWS mice (Stefan et al., 2011) and
396 the cell autonomous INS-1 model of PWS (this work) were associated with distinct
397 transcriptional responses. *In vivo*, an apparent physiological compensatory mechanism
398 increased levels of mRNAs encoding all major pancreatic hormones, including insulin,
399 amylin, glucagon, somatostatin, and PP, and several other secretory polypeptides (Stefan
400 et al., 2011). In contrast, in PWS INS-1 cell lines no changes in gene expression were
401 found for the endogenous rat *Ins1* or *Ins2* genes while there was diminished mRNA
402 expression of a *mIns2::mCherry* transgene and those encoding two other secreted
403 peptides (*Iapp* and *Npy*). Taken together, either translation or post-translational protein
404 folding and/or trafficking of insulins must be dysregulated in PWS β-cells.

405 A further critical finding in the PWS INS-1 model is a concurrent down-regulation
406 at the transcriptional and polypeptide levels of numerous ER chaperones, including for
407 GRP78 and GRP94 that are major facilitators of insulin folding and trafficking in the ER.
408 GRP94 directly binds pro-insulin, and chemical inhibition or shRNA knockdown or genetic
409 ablation of the *Hsp90b1* gene results in diminished insulin processing and secretion,
410 larger but immature insulin granules, and activation of the PERK ER stress pathway
411 (Ghiasi et al., 2019). Similarly, knockdown of *Hspa5* in INS-1(832/13) cells reduced insulin
412 biosynthesis and secretion (Zhang et al., 2009), a finding validated in human EndoC-βH1
413 cells (Szczerbinska et al., 2022). The acute reduction of single ER chaperones resulting
414 in reduced insulin production and secretion indicates a direct impact at the level of ER
415 insulin protein folding and trafficking that is recapitulated in the PWS INS-1 model where

416 we describe a chronic shortage of multiple ER-chaperones. Therefore, we interpret the
417 broad ER-chaperone deficiency in the PWS INS-1 model as a primary molecular
418 abnormality that directly results in diminished insulin secretion.

419 Prior evidence from mouse knockout models of key ER chaperone genes has
420 shown that they are subject to dosage compensation to maintain homeostasis. Although
421 knockouts for either *Hspa5* (GRP78) or *Hsp90b1* (GRP94) are lethal early in mouse
422 embryogenesis, heterozygous mice are viable (Luo et al., 2006; Mao et al., 2010; Ye et
423 al., 2010; Zhu and Lee, 2015). Intriguingly, upregulation of GRP94 and other ER
424 chaperones occurs in *Hspa5* +/- mice (Luo et al., 2006) and similarly for GRP78 in
425 *Hsp90b1* -/- ES cells (Mao et al., 2010), indicative of dosage compensation among ER
426 chaperones. A similar mechanism operates in *Hspa5* +/- mice to attenuate diet-induced
427 obesity and insulin resistance (Ye et al., 2010). Compensatory changes with upregulation
428 of GRP94 or GRP78 and other ER chaperones including PDIA6 also occurred with
429 shRNA knockdown of *Hspa5* or *Hsp90b1*, respectively, in a mouse cell line (Eletto et al.,
430 2012). In contrast, the widespread deficiency of ER chaperones, including GRP78 and
431 GRP94, that we describe for PWS INS-1 β-cells would preclude compensatory increases.
432 Because of an inability to compensate, we hypothesize that PWS β-cells have a chronic
433 deficit in ER chaperone production which would interfere with folding of proinsulin and/or
434 delay ER transit of cargo (e.g., hormones) along the secretory pathway. Consistent with
435 this hypothesis, our previous *in vivo* results using a Timer fluorescent protein
436 demonstrated an accumulation of aged insulin in islets of PWS mice (Stefan et al., 2011).

437 ER chaperones also function as sensors of ER stress, a physiological quality
438 control mechanism responding to accumulation or failure in degradation of misfolded
439 secretory proteins (Bertolotti et al., 2000; Braakman and Bulleid, 2011; Sun et al., 2015;

440 Tauber and Hoybye, 2021; Tiwari et al., 2013). ER stress responses, governed by the
441 IRE1α/XBP1, PERK/eIF2α/Ddit3(CHOP), and ATF6 regulatory pathways, aim to recover
442 ER homeostasis by upregulating ER chaperone gene expression as part of the UPR
443 (Bertolotti et al., 2000; Braakman and Bulleid, 2011; Sharma et al., 2021). In unstressed
444 cells, GRP78 forms stable complexes with each of IRE1α, PERK, and ATF6 in the ER
445 lumen (Bertolotti et al., 2000; Shen et al., 2002), whereas ER stress releases GRP78 and
446 induces each pathway. Due to the demand to fold high levels of insulin, a protein
447 notoriously difficult to fold (Sun et al., 2015), β-cells have a basal level of ATF6 activation
448 to maintain higher levels of GRP78 than for most cell types (Teodoro et al., 2012). In
449 contrast, unresolved ER stress within β-cells leads to diabetes in mouse models and
450 human (Salpea et al., 2020; Sharma et al., 2021). For example, insulin gene mutations
451 lead to insulin misfolding with induction of ER-stress and broad upregulation of the UPR
452 (Hartley et al., 2010), a converse mechanism to the reduced ER chaperone levels we
453 demonstrated within PWS INS-1 cells under both basal conditions and during GSIS.
454 Indeed, lower GRP78 levels in PWS β-cells likely accounts for the earlier and more robust
455 ER stress induction by thapsigargin or tunicamycin by lowering the threshold required to
456 dissociate ER stress activators resulting in cells that are poised to a greater degree for
457 response by all three master regulatory pathways. Although normal β-cells *in vivo* cycle
458 through states of elevated and low UPR coordinate with insulin gene expression and ER
459 protein folding load (Preissler and Ron, 2019; Sharma et al., 2015; Xin et al., 2018), our
460 omics data on steady-state mRNA and protein levels of bulk PWS INS-1 cells under basal
461 unstressed or GSIS conditions suggests a stress independent defect in ER chaperone
462 gene expression.

463 The coordinate downregulation of at least ten ER chaperone genes, including
464 *Hspa5* and *Hsp90b1*, in PWS β-cells, but not the whole suite of UPR genes, supports the
465 hypothesis that a PWS-imprinted gene or genes governs a pathway that coordinately
466 regulates ER chaperones in a unique gene regulatory network (GRN). Although many of
467 the DEGs that encode ER chaperones in PWS INS-1 β-cells are known ATF6 and/or
468 XBP1 targets, numerous ATF6, IRE1α/XBP1, and ATF4/CHOP (PERK pathway) target
469 genes (Acosta-Alvear et al., 2007; Adachi et al., 2008; Adamson et al., 2016; Belmont et
470 al., 2008; Bergmann et al., 2018; Park et al., 2021; Plate et al., 2016; Sharma et al., 2020;
471 Wiseman et al., 2022) are not dysregulated in PWS INS-1 lines, suggesting a novel GRN
472 in PWS β-cells. Candidate transcription factors (TFs) within the PWS-ER chaperone GRN
473 are those with binding site motifs enriched in the promoters of DEGs in PWS β-cells,
474 including, but not limited to the known ATF6 co-factor NFYA, which has roles in insulin
475 secretion and glucose homeostasis (Liu et al., 2021), as well as PPARB/D also with
476 known roles in β-cell mass and insulin secretion (Iglesias et al., 2012). Intriguingly, a
477 recently published study found that TFs of the nuclear receptor 4A (NR4A) family that
478 participate in long-term memory in mice act through coordinate regulation of numerous
479 ER chaperones (Chatterjee et al., 2022), with a high degree of concordance with the
480 dysregulated ER chaperones that we identified in PWS INS-1 cell lines; nevertheless,
481 NR4A pathway factors are not DEGs in PWS β-cells.

482 It also remains to be determined which PWS gene or genes regulates the putative
483 PWS→TF→ER chaperone network. Neither *Magel2* nor *Ndn* have a role, as they are not
484 expressed in INS-1 cells. The top candidate PWS genes that are highly expressed in INS-
485 1 cells are *Snrpn*, encoding the SmN spliceosomal protein (Gray et al., 1999b), *Snurf*,
486 encoding a small arginine-rich nuclear protein (Gray et al., 1999a), and *Snord116*, a

487 tandemly duplicated C/D-box snoRNA that may function as a sno-lncRNA that
488 sequestrates FOX2 and other RNA binding proteins in alternative splicing pathways (Wu
489 et al., 2016; Yin et al., 2012), or through direct binding and regulation of as yet undefined
490 RNA targets. Further studies are necessary to distinguish amongst the candidate PWS
491 genes and to identify downstream GRN steps leading to coordinated ER chaperone
492 expression.

493 Recent work has shown hypothalamic deficiencies in *Magel2*-null mice as well as
494 for iPSC- and dental-pulp stem cell neuronal models, specifically in secretory granule
495 components including PCSK1, PCSK2, CPE, granins (e.g., CHGB and others), and
496 numerous neuropeptides (Chen et al., 2020). These studies established that MAGEL2
497 plays a role in hypothalamic neuroendocrine cells by regulating neuropeptide production
498 and secretion via endosome recycling to prevent lysosomal degradation of secretory
499 granule proteins (Chen et al., 2020), a process downstream of the ER in protein trafficking
500 and secretory pathways. As discussed above, our study shows that another PWS-gene
501 (e.g., *Snrpn*, *Snurf*, and/or *Snord116*) is putatively responsible for regulating ER
502 chaperone and hormone (e.g., insulin) biosynthesis and secretion from pancreatic β-cells.
503 In contrast to the reported reduction of prohormone convertase PC1 in PWS iPSC-derived
504 neurons and in *Snord116*-null mice (Burnett et al., 2017), no deficiency in *Pcsk1* mRNA
505 or PC1/3 levels or in *Pcsk2* or PC2 was observed in PWS β-cell lines, which may reflect
506 differences in cell type, genetics, or experimental conditions. Combined, these
507 observations in hypothalamic neuroendocrine cells and pancreatic β-cells indicate that at
508 least two PWS-imprinted genes regulate related neuropeptide and peptide hormone
509 secretory pathways, suggesting that the PWS domain may function as a “mammalian

510 operon” or synexpression group (Nicholls, 1999; Niehrs and Pollet, 1999). As the PWS-
511 domain arose evolutionarily in a eutherian mammalian ancestor (Rapkins et al., 2006),
512 this suggests emergence of functions acting as molecular rheostats to regulate secretory
513 pathways in endocrine cells that control growth, metabolism, and neural pathways.

514 Maintaining glucose homeostasis relies on exquisite coordination between
515 secretion of the opposing hormones insulin and glucagon from pancreatic β- and α-cells,
516 respectively, in response to changes in blood glucose; disruption of these processes
517 contributes to the pathogenesis of metabolic disorders, including type 2 diabetes (T2D)
518 (Chen et al., 2018; Roder et al., 2016; Rorsman and Braun, 2013; Sandoval and
519 D'Alessio, 2015; Sharma et al., 2021). Although insulin and glucagon play opposite
520 regulatory roles both in normal metabolic homeostasis and dysfunction in T2D, PWS mice
521 are remarkable in having low blood levels of both insulin and glucagon (Stefan et al.,
522 2005; Stefan et al., 2011). As recent studies indicate that GRP78 interacts with glucagon
523 in α-cells (Asadi and Dhanvantari, 2018), it will be important to further assess
524 dysregulation of ER chaperones and glucagon secretion in PWS α-cells both in cell
525 culture and within PWS mouse models. Intriguingly, quantitative trait locus (QTL) studies
526 in mice link genetic variation in blood insulin and glucose levels in or near to the PWS-
527 orthologous domain (Lawson et al., 2011). Further studies are warranted to examine the
528 role of PWS-imprinted genes in these metabolic traits in humans, and whether β-cell or
529 other endocrine cell deficits in ER chaperones and hormone secretion contribute to
530 clinical phenotypes, including episodes of hypoglycemia in PWS subjects (Harrington et
531 al., 2014; Ma et al., 2012). As PWS genes regulate islet development, β- and α-cell
532 secretion (Schuster et al., 1996; Stefan et al., 2005; Stefan et al., 2011), and a GRN
533 affecting ER chaperone and insulin secretion (this study), identifying mechanisms by

534 which PWS-genes carry out these critical β-cell functions will illuminate the pathogenesis
535 and may reveal effective treatments for not only PWS, but for common disorders with
536 deficits in glycemic homeostasis and islet hormone secretory pathways.

537 **MATERIALS AND METHODS**

538

539 *Cell culture*

540 INS-1 lines were cultured using "RPMI 1640 media without glucose" (Life
541 Technologies) supplemented with 10% FBS, 10 mM HEPES, 1 mM sodium pyruvate,
542 0.05 mM 2-mercaptoethanol, 7.5 mM glucose, and antibiotics (1% Pen-Strep, 10 µg/ml
543 each piperacillin and ciprofloxacin). Chemical treatments included 0.1 µM thapsigargin
544 (Sigma) for either 5 hr or a 0-5 hr time-course, and 10 µg/ml tunicamycin (Sigma) for 5 hr
545 or a 0-8 hr time-course. The INS-1 lines used for genome editing in this study were
546 generated from parental INS-1(832/13) cells that have integrated a human *INS*-neoR
547 transgene (Hohmeier et al., 2000) as well as a mouse *Ins2*-C-mCherry transgene (Costa
548 RA, et al., manuscript in preparation).

549

550 *Genome editing*

551 Pairs of sgRNAs (**Table S6**) were designed (http://crispr.mit.edu/) to target sites
552 flanking the rodent PWS-orthologous domain to delete all paternally-expressed imprinted
553 genes (**Fig. 1A**), and cloned into the pX330 CRISPR/Cas9 vector (Ran et al., 2013)
554 (Addgene). INS-1 parental cells were transfected using lipofectamine 3000 with pX330-
555 vectors encoding sgRNAs targeting proximal of *Frat3* and distal (between *Snord115* and
556 *Ube3a*) of the PWS-domain and/or the control pEGFP-N3 vector (using 3 µg or 500 ng of
557 DNA per vector per T75 flask or 6-well plate, respectively). After 4 days culture at 30°C
558 or 37°C, cells were harvested for DNA isolation or flow cytometry (FACS ARIAII in the
559 Rangos Flow Cytometry Core Laboratory) with ~ 300 GFP-positive cells plated in five 96-
560 well plates and clonally expanded to 12-well plates for DNA isolation. Clonal lines were

561 screened by deletion-PCR and positive lines further expanded for DNA, RNA, protein,
562 and molecular cytogenetic analyses. PCR primers for deletion-PCR, inversion-PCR, and
563 scarred- or intact-allele PCRs are in **Table S7**. For DNA sequencing (Genewiz) of deletion
564 breakpoints and scarred or intact sgRNA sites, we Sanger sequenced PCR products
565 directly or from pJET (Thermo Fisher) cloned PCR products. Potential CRISPR/Cas9 off-
566 target sites were predicted *in silico* using CRISPOR (http://crispor.tefor.net/); top
567 predicted off-targets were PCR amplified (**Table S7**) and directly Sanger sequenced.
568
569 *Molecular cytogenetics*
570 Cytogenetic studies were carried out in the University of Pittsburgh Cell Culture
571 and Cytogenetics Facility. Briefly, cultured INS-1 cell lines were treated with 0.1 µg/ml
572 Colcemid 1 hr, harvested, fixed, and slides processed for metaphase FISH by standard
573 methods (Parikh et al., 2014). Fluorescent probes were prepared by labeling BAC
574 (BACPAC Genomics) DNA using nick translation (Enzo Life Sciences, Inc.), including
575 CH230-114P11 from the central PWS-domain (encodes U1A-*Snurf-Snrpn-Snord107-*
576 *Snord64*) with Orange-dUTP and control CH230-2B12 mapping several Mb distal of the
577 PWS domain (encodes *Cyfip1-Nipa2-Nipa1-Herc2*) with Green-dUTP. Probe and slide
578 preparation, hybridization, and DAPI staining were by standard cytogenetics methods,
579 with FISH analyses on an Olympus BX61 epifluorescence microscope (Olympus
580 Microscopes) and image capture and analysis using the Genus software platform on the
581 Cytovision System (Leica Microsystems) (Parikh et al., 2014).
582
583 *Droplet digital PCR (ddPCR) genomic copy number assays*
584 For genomic copy number 5 ng of *EcoR*I digested genomic DNA was used as input

585 with amplification of *Snord107*, PWS-IC, and *Mirh1* as targets and *Ube3a* as a reference;
586 during clonal derivatization EvaGreen chemistry was used whereas Fam/Hex TaqMan
587 probes were used in a final analysis. Absolute copy number of *Snord107* and Poisson
588 confidence intervals were calculated by numerical approximation (Dube et al., 2008).
589 Primers and probes for copy number ddPCR are listed in **Table S7**.
590
591 *DNA methylation*
592 Genomic DNA was bisulfite converted using the EZ DNA methylation Gold kit
593 (Zymo Research). Outer first round genomic PCR was performed using primers to amplify
594 the *Snurf-Snrpn* promoter region (annealing temperature or Ta of 64°C; **Table S7**), with
595 subsequent second round genomic PCR performed using PCR primers specific for the
596 maternal, methylated or paternal, unmethylated alleles (Ta of 60°C; **Table S7**). HotStart
597 Taq polymerase (Qiagen) was used for all methylation PCR.
598
599 *Insulin secretion assays*
600 Cells were plated at 1.0 x 10^6 cells/well, then 24 hr later at ~ 80% confluency were
601 washed with PBS containing Mg^{++} and Ca^{++} (Gibco), pre-incubated 1.0 hr in KRBH (129
602 mM NaCl, 5 mM $NaHCO_3$, 4.8 mM KCl, 1.2 mM $KH2PO_4$, 1.2 mM $MgSO_4$, 2.5 mM $CaCl_2$,
603 10 mM HEPES, 0.1% BSA) with low glucose (LG; 2.8 mM) and washed in KRBH (without
604 glucose). Following a 30 min incubation in KRBH-LG, 1.0 ml low glucose secreted
605 fractions were removed and centrifuged 13,000 rpm for 5 min., aliquoted and stored at -
606 80°C. The cells were then incubated 30 min in KRBH-high glucose (HG; 22 mM), and
607 high glucose secreted fractions similarly centrifuged and stored at -80°C. Finally, cells
608 were washed in PBS containing Mg^{++} and Ca^{++}, harvested in RIPA lysis buffer and

609 protease inhibitor, centrifuged at 13,000 rpm for 15 min at 4°C and the supernatant
610 (protein) stored at -80°C. Protein was determined using Pierce BCA protein assay kit
611 (Thermo Fisher). Insulin was measured by the RIA and Biomarkers Core of the Penn
612 Diabetes Research Center, University of Pennsylvania, using an ultrasensitive rat insulin
613 ELISA kit (Alpco Diagnostics). ANOVA followed by the Tukey HSD post-hoc test was
614 used to assess differences between different conditions and genotypes using Prism 8
615 (GraphPad Software, Inc).
616
617 *Reverse transcription-PCR*
618 Total RNA was isolated from PWS and control INS-1 lines grown as above (7.5
619 mM glucose) by Trizol harvest and miRNeasy (Qiagen) column purification. RNA quality
620 was assessed by RNA TapeStation (Agilent) and quantified by broad range Qubit
621 (Thermo Fisher) fluorometric analysis. First strand cDNA synthesis from 1 µg RNA was
622 carried out using random hexamer primed RT by using Super Script IV (Thermo Fisher).
623 Primers for gene specific RT-PCR amplification are in **Table S8**.
624
625 *RT-Droplet digital-PCR (RT-ddPCR) assays*
626 Template cDNA pools were generated from 1 µg RNA using cells grown under
627 standard glucose conditions (as above) by using iScript (Bio-Rad) RT with first-strand
628 synthesis priming from a mixture of random hexamers and oligo-dT. Droplet generation,
629 PCR and reading of EvaGreen based ddPCR reactions was carried out using an
630 automated QX200 ddPCR system (Bio-Rad). A total template input volume of 2 µl of
631 cDNA diluted in a range from undiluted to 1:200 (30 ng to 0.15 ng RNA equivalents per
632 reaction) determined empirically based on the absolute expression level of target genes

633 was used per 20 µl reaction. Primer sequences are listed in **Table S8**. Expression of
634 target genes was normalized to the stable and modestly expressed *Gpi* (1:5 diluted, 6.0
635 ng RNA equivalents) as the ratio of positive droplet concentration and normalized to the
636 average expression levels of target genes in the control INS-1 lines. Relative expression
637 of target genes in PWS and control lines was compared using the Welch's t-test for
638 unequal variance with a significant threshold of $P < 0.05$.
639
640 *Proteomics*
641 Each of the 3 control cell lines (5-9, 2, 16) and the 3 PWS cell lines (3, 19-1, 19-4)
642 were grown in 6-well plates, harvested and then washed with PBS containing Mg^{++} and
643 Ca^{++}, incubated 30 min in KRH-high glucose (22 mM, glucose-induced insulin secretion
644 condition, with BSA excluded from the KRBH buffer) after which the media was collected,
645 centrifuged 10 min 1300 rpm, and supernatant (secretory fractions 1-6; **Fig. 3A**) collected
646 and stored at -80°C. Cellular proteins were harvested by direct addition of 1.0 ml of
647 methanol-acetic acid (90% methanol, 9% water, 1% acetic acid) to each well, transferred
648 to a microcentrifuge tube and centrifuged at 1300 rpm 15 min. The supernatant (soluble
649 protein fractions 7-12; **Fig. 3A**) and pellets (insoluble protein fractions 13-18; **Fig. 3A**)
650 were collected and stored at -80°C. The secretory and cellular fractions were dried *in*
651 *vacuo* and stored at -80°C. In preparation for mass spectrometry, proteins from each
652 fraction were dissolved in 8 M urea, 100 µM Triethylammonium bicarbonate (TEAB) pH
653 8.5, reduced with tris(2-carboxyethyl)phosphine (TCEP) and alkylated with
654 chloroacetamide, then diluted to 2 M urea with 100 mM TEAB, addition of 0.5 µg trypsin
655 (Promega) and placed in a 37°C shaker for 16 hrs. Secretory protein fractions were
656 analyzed on an Orbitrap Elite mass spectrometer (Thermo Fisher) while cellular protein

657 fractions were analyzed on an Orbitrap Fusion mass spectrometer (Thermo Fisher). The
658 6-plex Tandem Mass Tag (TMT) system for quantitative proteomics (Thermo Fisher) was
659 used to compare methanol-acetic acid insoluble cellular proteins (fractions 13-18) for
660 control and PWS cell lines. The TMT labeled samples were analyzed on an Orbitrap
661 Fusion Lumos mass spectrometer (Thermo Fisher).

662 Peptide/protein identification and quantification were determined using IP2
663 (Integrated Proteomics Applications). The MS raw data files were converted using
664 RawConverter (He et al., 2015) (version 1.1.0.23) with monoisotopic option. For peptide
665 identification, tandem mass spectra were searched against a database including the
666 UniProt Rat database one entry per gene (21589 entries released 5/30/2021), these
667 entries scrambled between K and R to make a decoy database, common contaminants,
668 peptides and custom proteins using ProLuCID (Xu et al., 2015), and data filtered using
669 DTASelect (Tabb et al., 2002). Quantitation of TMT samples was calculated with Census
670 version 2.51 (Park et al., 2014) and filtered with an intensity value of 5000 and isobaric
671 purity value of 0.6 (Sandberg et al., 2014). The Quantitative@COMPARE feature of IP2
672 was used to determine statistical significance.

673

674 *Immunoblot analyses*

675 Cells were grown under standard glucose conditions with or without the addition
676 of DMSO, thapsigargin or tunicamycin (as above). Whole cell lysates were harvested by
677 direct lysis in cold radioimmunoprecipitation buffer (RIPA) with the addition of EDTA and
678 combined protease and phosphatase inhibitors (Thermo Fisher) followed by clearing of
679 insoluble material by centrifugation at 13,000 RPM for 10 minutes. Proteins were
680 separated by SDS-PAGE with 2-mercaptoethanol as a reducing agent using criterion

681 sized 4-15% gradient tris-glycine for broad range of molecular weights greater than 30
682 kDa or 16.5% tris-tricine for high resolution of smaller proteins (Bio-Rad). Proteins were
683 transferred to nitrocellulose membranes and probed with antibodies [commercially
684 obtained except for ATF6 (Teske et al., 2011), with dilutions as in **Table S9**].
685 Chemiluminescence detection of HRP-conjugated secondary antibodies was performed
686 with either Clarity or Clarity Max Western ECL detection kits on a Bio-Rad Chemi-Doc
687 XRS+ imager. Densitometry measurements were made using Image Lab (Bio-Rad)
688 software and exported for analysis in R. Statistical comparison of normalized protein
689 levels between PWS and control samples was made by either Welch's unequal variance
690 t-test or by ANOVA with Tukey's HSD post-hoc test for multiple comparison where
691 appropriate, with a significance threshold of $P < 0.05$.
692
693 *Transmission electron microscopy*
694 Monolayers of INS-1 cells were fixed in 2.5% glutaraldehyde in 100 mM PBS, post-
695 fixed in aqueous 1% osmium tetroxide, 1% Fe_6CN_3 for 1 hr, and dehydrated prior to
696 embedding in Polybed 812 resin (Polysciences). Ultrathin cross sections (60 nm) of the
697 cells were obtained on a Riechart Ultracut E microtome, post-stained in 4% uranyl acetate
698 for 10 min and 1% lead citrate for 7 min. Sections were viewed on a JEOL JEM 1400
699 FLASH transmission electron microscope (JEOL) at 80 KV. Images were taken using a
700 bottom mount AMT digital camera (Advanced Microscopy Techniques).
701
702 *Confocal microscopy*
703 For each of the 3 control and 3 PWS INS-1 lines 750,000 live cells were seeded
704 on a 35 mm dish with an uncoated 14 mm glass bottom insert (Mattek) and allowed to

705 grow for 36 hr in basal glucose conditions. Live cell imaging was performed on a Zeiss
706 LSM 710 confocal microscope at 20x magnification to capture mCherry fluorescence and
707 brightfield images.
708
709 *RNA-seq and bioinformatics*
710 Total RNA (from cells grown under 7.5 mM glucose) was used to prepare rRNA
711 depleted Illumina TruSeq 75-bp paired-end stranded (fr-firststrand) sequencing libraries
712 and sequenced to a depth of ~ 40 million reads on a NextSeq500 instrument at the UPMC
713 Children's Hospital of Pittsburgh Genomics Core. RNA-seq data analysis was performed
714 using computational resources available from the University of Pittsburgh Center for
715 Research Computing. Quality of reads was assessed by FastQC and sequencing
716 adapters trimmed by cutadapt using the combined TrimGalore tool (Krueger, 2015). The
717 sequencing reads were aligned to the Ensembl v98 rat genome to which the sequence
718 and annotation of the human *INS*-neo^{R} and mouse *Ins2*-C-mCherry transgenes had been
719 added along with annotation of previously undefined genomic features (e.g., *Ipw*, *ψSnurf*,
720 and upstream *U1 Snurf-Snrpn* exons) using the STAR splice-aware aligner (Dobin et al.,
721 2013). Gene feature counts were tabulated with HTSeq using either the default (--
722 nonunique none) or customized (--nonunique all) options to enable the inclusion of multi-
723 copy (i.e., *Snord116*) and overlapping (bicistronic *Snurf-Snrpn*) genes which otherwise
724 were excluded as ambiguous reads under the default options (Anders et al., 2015).
725 Differential expression analysis was performed with DESeq2 using a cutoff of *P*adj < 0.1
726 as calculated by the Benjamini-Hochberg multiple comparison procedure (Love et al.,
727 2014). Similar overall transcriptomic results were obtained with RSEM based analysis (Li
728 and Dewey, 2011) but had lower counts for both multi-mapped reads for *Snord116* and

729 for ambiguous bicistronic *Snurf-Snrpn* reads. Gene ontology enrichment analysis of up-
730 and down-regulated gene sets was done using DAVID (Dennis et al., 2003). Additional
731 gene ontology and upstream analysis utilized Enrichr (Chen et al., 2013).

732 Sequencing libraries of small RNAs including snoRNAs were made from the same
733 total RNA isolation but using a miRNA-Seq (Qiagen) library prep kit with a modified size
734 selection for up to 200-bp fragments. Single end reads were generated and sequenced.
735 UMI tools (Smith et al., 2017) and Cutadapt (Martin, 2011) were used to deduplicate and
736 remove adapters in preprocessing of the fastq reads for alignment with Bowtie2
737 (Langmead and Salzberg, 2012). Similar to the total RNA-seq, HTSeq required the --
738 nonunique all option to accurately quantitate the multicopy snoRNA and miRNA genes,
739 and DESeq2 was used for differential expression analysis to compare genotypes. A full
740 set of bash scripts for analysis of both total and small RNA-seq data sets including custom
741 annotations are provided at the github repository (https://github.com/KoppesEA/INS-
742 1_PWS_RNA-Seq).

743 **DATA STATEMENT**

744 The RNA-seq FASTQ files and processed data associated from this study have
745 been deposited in the NCBI Gene Expression Omnibus (GEO) under SuperSeries
746 GSE190337 including GSE190334 (total RNA-seq) and GSE190336 (small RNA-seq),
747 assigned to BioProject PRJNA786769.

748 The TMT quantitative proteomics data files have been deposited at
749 ProteomeXchange under accession number PXD#.

750

751 **ACKNOWLEDGMENTS**

752 We thank Dr. Michael R. Rickels and Heather W. Collins at the Penn Diabetes
753 Center RIA/Biomarkers Core, Mary F. Sanchirico for the protein database, Dr. Régis A.
754 Costa for off-target PCR primer design, and Drs. Rebecca A. Simmons and Dwi
755 Kemaladewi for review of the manuscript. This project used the University of Pittsburgh
756 Health Sciences Sequencing Core at UPMC Children's Hospital of Pittsburgh, for RNA
757 sequencing. This work was supported by a research grant to R.D.N. from the Foundation
758 for Prader-Willi Research (FPWR) and funding to R.D.N. from the Storr Family
759 Foundation through the Prader-Willi Syndrome Association (PWSA). J.J.M., J.K.D., and
760 J.R.Y. were supported by the National Institute of General Medical Sciences (8P41
761 GM103533). This manuscript is dedicated to PWS families and especially the Storr family
762 for their support of our PWS research program.

763

764 **AUTHOR CONTRIBUTIONS**

765 EAK, MAJ, JJM, PL, DWL, DBS, JKD performed experiments and analyzed data;
766 EAK performed bioinformatics analyses; EAK, JJM, DBS, JRY, SCW, SMG, HJP, PD,

767 RDN designed experiments and interpreted data; RCW provided a critical reagent; EAK,
768 RDN wrote the manuscript; all co-authors reviewed and approved manuscript drafts and
769 final version.
770
771 **CONFLICT OF INTEREST**
772 None declared.
773

774 **REFERENCES**

775

776 Acosta-Alvear, D., Zhou, Y., Blais, A., Tsikitis, M., Lents, N.H., Arias, C., Lennon, C.J.,
777 Kluger, Y., and Dynlacht, B.D. (2007). XBP1 controls diverse cell type- and condition-
778 specific transcriptional regulatory networks. Mol Cell *27*, 53-66.
779
780 Adachi, Y., Yamamoto, K., Okada, T., Yoshida, H., Harada, A., and Mori, K. (2008). ATF6
781 is a transcription factor specializing in the regulation of quality control proteins in the
782 endoplasmic reticulum. Cell Struct Funct *33*, 75-89.
783
784 Adamson, B., Norman, T.M., Jost, M., Cho, M.Y., Nunez, J.K., Chen, Y., Villalta, J.E.,
785 Gilbert, L.A., Horlbeck, M.A., Hein, M.Y., et al. (2016). A multiplexed single-cell CRISPR
786 screening platform enables systematic dissection of the unfolded protein response. Cell
787 *167*, 1867-1882 e1821.
788
789 Anders, S., Pyl, P.T., and Huber, W. (2015). HTSeq--a Python framework to work with
790 high-throughput sequencing data. Bioinformatics *31*, 166-169.
791
792 Asadi, F., and Dhanvantari, S. (2018). Plasticity in the glucagon interactome reveals novel
793 proteins that regulate glucagon secretion in α-TC1-6 cells. Front Endocrinol *9*, 792.
794
795 Belmont, P.J., Tadimalla, A., Chen, W.J., Martindale, J.J., Thuerauf, D.J., Marcinko, M.,
796 Gude, N., Sussman, M.A., and Glembotski, C.C. (2008). Coordination of growth and
797 endoplasmic reticulum stress signaling by regulator of calcineurin 1 (RCAN1), a novel
798 ATF6-inducible gene. J Biol Chem *283*, 14012-14021.
799
800 Benner, C., van der Meulen, T., Caceres, E., Tigyi, K., Donaldson, C.J., and Huising, M.O.
801 (2014). The transcriptional landscape of mouse beta cells compared to human beta cells
802 reveals notable species differences in long non-coding RNA and protein-coding gene
803 expression. BMC Genomics *15*, 620.
804
805 Bergmann, T.J., Fregno, I., Fumagalli, F., Rinaldi, A., Bertoni, F., Boersema, P.J., Picotti,
806 P., and Molinari, M. (2018). Chemical stresses fail to mimic the unfolded protein response
807 resulting from luminal load with unfolded polypeptides. J Biol Chem *293*, 5600-5612.
808
809 Bertolotti, A., Zhang, Y., Hendershot, L.M., Harding, H.P., and Ron, D. (2000). Dynamic
810 interaction of BiP and ER stress transducers in the unfolded-protein response. Nat Cell
811 Biol *2*, 326-332.
812
813 Braakman, I., and Bulleid, N.J. (2011). Protein folding and modification in the mammalian
814 endoplasmic reticulum. Annu Rev Biochem *80*, 71-99.
815
816 Burnett, L.C., LeDuc, C.A., Sulsona, C.R., Paull, D., Rausch, R., Eddiry, S., Carli, J.F.,
817 Morabito, M.V., Skowronski, A.A., Hubner, G., et al. (2017). Deficiency in prohormone
818 convertase PC1 impairs prohormone processing in Prader-Willi syndrome. J Clin Invest
819 *127*, 293-305.

820
821 Castle, J.C., Armour, C.D., Lower, M., Haynor, D., Biery, M., Bouzek, H., Chen, R.,
822 Jackson, S., Johnson, J.M., Rohl, C.A., and Raymond, C.K. (2010). Digital genome-wide
823 ncRNA expression, including snoRNAs, across 11 human tissues using polyA-neutral
824 amplification. PLoS One *5*, e11779.
825
826 Cavaillé, J., Buiting, K., Kiefmann, M., Lalande, M., Brannan, C.I., Horsthemke, B.,
827 Bachellerie, J.P., Brosius, J., and Hüttenhofer, A. (2000). Identification of brain-specific
828 and imprinted small nucleolar RNA genes exhibiting an unusual genomic organization.
829 Proc Natl Acad Sci U S A *97*, 14311-14316.
830
831 Chatterjee, S., Bahl, E., Mukherjee, U., Walsh, E.N., Shetty, M.S., Yan, A.L., Vanrobaeys,
832 Y., Lederman, J.D., Giese, K.P., Michaelson, J., and Abel, T. (2022). Endoplasmic
833 reticulum chaperone genes encode effectors of long-term memory. Sci Adv *8*, eabm6063.
834
835 Chen, E.Y., Tan, C.M., Kou, Y., Duan, Q., Wang, Z., Meirelles, G.V., Clark, N.R., and
836 Ma'ayan, A. (2013). Enrichr: interactive and collaborative HTML5 gene list enrichment
837 analysis tool. BMC Bioinformatics *14*, 128.
838
839 Chen, H., Victor, A.K., Klein, J., Tacer, K.F., Tai, D.J., de Esch, C., Nuttle, A., Temirov,
840 J., Burnett, L.C., Rosenbaum, M., et al. (2020). Loss of MAGEL2 in Prader-Willi syndrome
841 leads to decreased secretory granule and neuropeptide production. JCI Insight *5*,
842 e138576.
843
844 Chen, Y.C., Taylor, A.J., and Verchere, C.B. (2018). Islet prohormone processing in
845 health and disease. Diabetes Obes Metab *20 Suppl 2*, 64-76.
846
847 Chung, M.S., Langouet, M., Chamberlain, S.J., and Carmichael, G.G. (2020). Prader-Willi
848 syndrome: reflections on seminal studies and future therapies. Open Biol *10*, 200195.
849
850 Cnop, M., Abdulkarim, B., Bottu, G., Cunha, D.A., Igoillo-Esteve, M., Masini, M.,
851 Turatsinze, J.V., Griebel, T., Villate, O., Santin, I., et al. (2014). RNA sequencing identifies
852 dysregulation of the human pancreatic islet transcriptome by the saturated fatty acid
853 palmitate. Diabetes *63*, 1978-1993.
854
855 Costa, R.A., Ferreira, I.R., Cintra, H.A., Gomes, L.H.F., and Guida, L.D.C. (2019).
856 Genotype-phenotype relationships and endocrine findings in Prader-Willi syndrome.
857 Front Endocrinol *10*, 864.
858
859 Cummings, D.E., Clement, K., Purnell, J.Q., Vaisse, C., Foster, K.E., Frayo, R.S.,
860 Schwartz, M.W., Basdevant, A., and Weigle, D.S. (2002). Elevated plasma ghrelin levels
861 in Prader Willi syndrome. Nat Med *8*, 643-644.
862
863 Deal, C.L., Tony, M., Höybye, C., Allen, D.B., Tauber, M., Christiansen, J.S., and Growth
864 Hormone in Prader-Willi Syndrome Clinical Care Guidelines Workshop Participants.
865 (2013). Growth Hormone Research Society workshop summary: consensus guidelines

for recombinant human growth hormone therapy in Prader-Willi syndrome. J Clin Endocrinol Metab *98*, E1072-1087.

Dennis, G., Jr., Sherman, B.T., Hosack, D.A., Yang, J., Gao, W., Lane, H.C., and Lempicki, R.A. (2003). DAVID: Database for Annotation, Visualization, and Integrated Discovery. Genome Biol *4*, P3.

Dobin, A., Davis, C.A., Schlesinger, F., Drenkow, J., Zaleski, C., Jha, S., Batut, P., Chaisson, M., and Gingeras, T.R. (2013). STAR: ultrafast universal RNA-seq aligner. Bioinformatics *29*, 15-21.

Drujont, L., Lemoine, A., Moreau, A., Bienvenu, G., Lancien, M., Cens, T., Guillot, F., Bériou, G., Bouchet-Delbos, L., Fehling, H.J., et al. (2016). RORγt+ cells selectively express redundant cation channels linked to the Golgi apparatus. Sci Rep *6*, 23682.

Dube, S., Qin, J., and Ramakrishnan, R. (2008). Mathematical analysis of copy number variation in a DNA sample using digital PCR on a nanofluidic device. PLoS One *3*, e2876.

Eizirik, D.L., Sammeth, M., Bouckenooghe, T., Bottu, G., Sisino, G., Igoillo-Esteve, M., Ortis, F., Santin, I., Colli, M.L., Barthson, J., et al. (2012). The human pancreatic islet transcriptome: expression of candidate genes for type 1 diabetes and the impact of pro-inflammatory cytokines. PLoS Genet *8*, e1002552.

Eletto, D., Maganty, A., Eletto, D., Dersh, D., Makarewich, C., Biswas, C., Paton, J.C., Paton, A.W., Doroudgar, S., Glembotski, C.C., and Argon, Y. (2012). Limitation of individual folding resources in the ER leads to outcomes distinct from the unfolded protein response. J Cell Sci *125*, 4865-4875.

Fan, F., Matsunaga, K., Wang, H., Ishizaki, R., Kobayashi, E., Kiyonari, H., Mukumoto, Y., Okunishi, K., and Izumi, T. (2017). Exophilin-8 assembles secretory granules for exocytosis in the actin cortex via interaction with RIM-BP2 and myosin-VIIa. Elife *6*, e26174.

Fountain, M.D., Jr., and Schaaf, C.P. (2015). MAGEL2 and oxytocin-implications in Prader-Willi syndrome and beyond. Biol Psychiatry *78*, 78-80.

Fujimoto, K., Shibasaki, T., Yokoi, N., Kashima, Y., Matsumoto, M., Sasaki, T., Tajima, N., Iwanaga, T., and Seino, S. (2002). Piccolo, a Ca2+ sensor in pancreatic beta-cells. Involvement of cAMP-GEFII.Rim2. Piccolo complex in cAMP-dependent exocytosis. J Biol Chem *277*, 50497-50502.

Ghiasi, S.M., Dahlby, T., Hede Andersen, C., Haataja, L., Petersen, S., Omar-Hmeadi, M., Yang, M., Pihl, C., Bresson, S.E., Khilji, M.S., et al. (2019). Endoplasmic reticulum chaperone glucose-regulated protein 94 is essential for proinsulin handling. Diabetes *68*, 747-760.

912 Goldstone, A.P., Patterson, M., Kalingag, N., Ghatei, M.A., Brynes, A.E., Bloom, S.R.,
913 Grossman, A.B., and Korbonits, M. (2005). Fasting and postprandial hyperghrelinemia in
914 Prader-Willi syndrome is partially explained by hypoinsulinemia, and is not due to peptide
915 YY3-36 deficiency or seen in hypothalamic obesity due to craniopharyngioma. J Clin
916 Endocrinol Metab *90*, 2681-2690.
917
918 Gray, T.A., Saitoh, S., and Nicholls, R.D. (1999a). An imprinted, mammalian bicistronic
919 transcript encodes two independent proteins. Proc Natl Acad Sci U S A *96*, 5616-5621.
920
921 Gray, T.A., Smithwick, M.J., Schaldach, M.A., Martone, D.L., Graves, J.A., McCarrey,
922 J.R., and Nicholls, R.D. (1999b). Concerted regulation and molecular evolution of the
923 duplicated SNRPB'/B and SNRPN loci. Nucleic Acids Res *27*, 4577-4584.
924
925 Harrington, R.A., Weinstein, D.A., and Miller, J.L. (2014). Hypoglycemia in Prader-Willi
926 syndrome. Am J Med Genet A *164A*, 1127-1129.
927
928 Hartley, T., Siva, M., Lai, E., Teodoro, T., Zhang, L., and Volchuk, A. (2010). Endoplasmic
929 reticulum stress response in an INS-1 pancreatic beta-cell line with inducible expression
930 of a folding-deficient proinsulin. BMC Cell Biol *11*, 59.
931
932 He, L., Diedrich, J., Chu, Y.Y., and Yates, J.R., 3rd (2015). Extracting accurate precursor
933 information for tandem mass spectra by RawConverter. Anal Chem *87*, 11361-11367.
934
935 Hirsch, H.J., Eldar-Geva, T., Bennaroch, F., Pollak, Y., and Gross-Tsur, V. (2015). Sexual
936 dichotomy of gonadal function in Prader-Willi syndrome from early infancy through the
937 fourth decade. Hum Reprod *30*, 2587-2596.
938
939 Hohmeier, H.E., Mulder, H., Chen, G., Henkel-Rieger, R., Prentki, M., and Newgard, C.B.
940 (2000). Isolation of INS-1-derived cell lines with robust ATP-sensitive K+ channel-
941 dependent and -independent glucose-stimulated insulin secretion. Diabetes *49*, 424-430.
942
943 Hong, M., Luo, S., Baumeister, P., Huang, J.M., Gogia, R.K., Li, M., and Lee, A.S. (2004).
944 Underglycosylation of ATF6 as a novel sensing mechanism for activation of the unfolded
945 protein response. J Biol Chem *279*, 11354-11363.
946
947 Iglesias, J., Barg, S., Vallois, D., Lahiri, S., Roger, C., Yessoufou, A., Pradevand, S.,
948 McDonald, A., Bonal, C., Reimann, F., et al. (2012). PPARβ/δ affects pancreatic β cell
949 mass and insulin secretion in mice. J Clin Invest *122*, 4105-4117.
950
951 Kalwat, M.A., Scheuner, D., Rodrigues-Dos-Santos, K., Eizirik, D.L., and Cobb, M.H.
952 (2021). The pancreatic β-cell response to secretory demands and adaption to stress.
953 Endocrinology *162*, bqab173.
954
955 Kishore, S., and Stamm, S. (2006). The snoRNA HBII-52 regulates alternative splicing of
956 the serotonin receptor 2C. Science *311*, 230-232.
957

958 Krishnan, P., Syed, F., Jiyun Kang, N., Mirmira, R.G., and Evans-Molina, C. (2019).
959 Profiling of RNAs from human islet-derived exosomes in a model of type 1 diabetes. Int J
960 Mol Sci *20*, 5903.
961
962 Kronenberg-Versteeg, D., Eichmann, M., Russell, M.A., de Ru, A., Hehn, B., Yusuf, N.,
963 van Veelen, P.A., Richardson, S.J., Morgan, N.G., Lemberg, M.K., and Peakman, M.
964 (2018). Molecular pathways for immune recognition of preproinsulin signal peptide in type
965 1 diabetes. Diabetes *67*, 687-696.
966
967 Krueger, F. (2015). Trim galore: A wrapper tool around Cutadapt and FastQC to
968 consistently apply quality and adapter trimming to fastq files.
969 http://www.bioinformatics.babraham.ac.uk/projects/trim_galore/.
970
971 Langmead, B., and Salzberg, S.L. (2012). Fast gapped-read alignment with Bowtie 2. Nat
972 Methods *9*, 357-359.
973
974 Lawlor, N., Marquez, E.J., Orchard, P., Narisu, N., Shamim, M.S., Thibodeau, A.,
975 Varshney, A., Kursawe, R., Erdos, M.R., Kanke, M., et al. (2019). Multiomic profiling
976 identifies cis-regulatory networks underlying human pancreatic β cell identity and
977 function. Cell Rep *26*, 788-801.
978
979 Lawson, H.A., Lee, A., Fawcett, G.L., Wang, B., Pletscher, L.S., Maxwell, T.J., Ehrich,
980 T.H., Kenney-Hunt, J.P., Wolf, J.B., Semenkovich, C.F., and Cheverud, J.M. (2011). The
981 importance of context to the genetic architecture of diabetes-related traits is revealed in
982 a genome-wide scan of a LG/J x SM/J murine model. Mamm Genome *22*, 197-208.
983
984 Lee, H.J., Choe, Y.H., Lee, J.H., Sohn, Y.B., Kim, S.J., Park, S.W., Son, J.S., Kim, S.W.,
985 and Jin, D.K. (2011). Delayed response of amylin levels after an oral glucose challenge
986 in children with Prader-Willi syndrome. Yonsei Med J *52*, 257-262.
987
988 Li, B., and Dewey, C.N. (2011). RSEM: accurate transcript quantification from RNA-Seq
989 data with or without a reference genome. BMC Bioinformatics *12*, 323.
990
991 Li, J., Klughammer, J., Farlik, M., Penz, T., Spittler, A., Barbieux, C., Berishvili, E., Bock,
992 C., and Kubicek, S. (2016a). Single-cell transcriptomes reveal characteristic features of
993 human pancreatic islet cell types. EMBO Rep *17*, 178-187.
994
995 Li, L., Pan, Z.F., Huang, X., Wu, B.W., Li, T., Kang, M.X., Ge, R.S., Hu, X.Y., Zhang, Y.H.,
996 Ge, L.J., et al. (2016b). Junctophilin 3 expresses in pancreatic beta cells and is required
997 for glucose-stimulated insulin secretion. Cell Death Dis *7*, e2275.
998
999 Liu, Q., He, H., Zeng, T., Huang, Z., Fan, T., and Wu, Q. (2014). Neural-specific
1000 expression of miR-344-3p during mouse embryonic development. J Mol Histol *45*, 363-
1001 372.
1002

1003 Liu, Y., He, S., Zhou, R., Zhang, X., Yang, S., Deng, D., Zhang, C., Yu, X., Chen, Y., and
1004 Su, Z. (2021). Nuclear factor-Y in mouse pancreatic β-cells plays a crucial role in glucose
1005 homeostasis by regulating β-cell mass and insulin secretion. Diabetes *70*, 1703-1716.
1006
1007 Love, M.I., Huber, W., and Anders, S. (2014). Moderated estimation of fold change and
1008 dispersion for RNA-seq data with DESeq2. Genome Biol *15*, 550.
1009
1010 Low, B.S.J., Lim, C.S., Ding, S.S.L., Tan, Y.S., Ng, N.H.J., Krishnan, V.G., Ang, S.F.,
1011 Neo, C.W.Y., Verma, C.S., Hoon, S., et al. (2021). Decreased GLUT2 and glucose uptake
1012 contribute to insulin secretion defects in MODY3/HNF1A hiPSC-derived mutant β cells.
1013 Nat Commun *12*, 3133.
1014
1015 Luo, S., Mao, C., Lee, B., and Lee, A.S. (2006). GRP78/BiP is required for cell
1016 proliferation and protecting the inner cell mass from apoptosis during early mouse
1017 embryonic development. Mol Cell Biol *26*, 5688-5697.
1018
1019 Ma, Y., Wu, T., Liu, Y., Wang, Q., Song, J., Song, F., and Yang, Y. (2012). Nutritional and
1020 metabolic findings in patients with Prader-Willi syndrome diagnosed in early infancy. J
1021 Pediatr Endocrinol Metab *25*, 1103-1109.
1022
1023 Mao, C., Wang, M., Luo, B., Wey, S., Dong, D., Wesselschmidt, R., Rawlings, S., and
1024 Lee, A.S. (2010). Targeted mutation of the mouse Grp94 gene disrupts development and
1025 perturbs endoplasmic reticulum stress signaling. PLoS One *5*, e10852.
1026
1027 Martin, M. (2011). Cutadapt removes adapter sequences from high-throughput
1028 sequencing reads. EMBnet.journal *17*, 3.
1029
1030 Matsunaga, K., Taoka, M., Isobe, T., and Izumi, T. (2017). Rab2a and Rab27a
1031 cooperatively regulate the transition from granule maturation to exocytosis through the
1032 dual effector Noc2. J Cell Sci *130*, 541-550.
1033
1034 Muscogiuri, G., Formoso, G., Pugliese, G., Ruggeri, R.M., Scarano, E., Colao, A., and
1035 RESTARE (2019). Prader-Willi syndrome: An uptodate on endocrine and metabolic
1036 complications. Rev Endocr Metab Disord *20*, 239-250.
1037
1038 Naito, T., Takatsu, H., Miyano, R., Takada, N., Nakayama, K., and Shin, H.W. (2015).
1039 Phospholipid flippase ATP10A translocates phosphatidylcholine and is involved in
1040 plasma membrane dynamics. J Biol Chem *290*, 15004-15017.
1041
1042 Nakajima-Nagata, N., Sugai, M., Sakurai, T., Miyazaki, J., Tabata, Y., and Shimizu, A.
1043 (2004). Pdx-1 enables insulin secretion by regulating synaptotagmin 1 gene expression.
1044 Biochem Biophys Res Commun *318*, 631-635.
1045
1046 Nicholls, R.D. (1999). Incriminating gene suspects, Prader-Willi style. Nat Genet *23*, 132-
1047 134.
1048

1049 Nicholls, R.D., and Knepper, J.L. (2001). Genome organization, function, and imprinting
1050 in Prader-Willi and Angelman syndromes. Annu Rev Genomics Hum Genet *2*, 153-175.
1051
1052 Niehrs, C., and Pollet, N. (1999). Synexpression groups in eukaryotes. Nature *402*, 483-
1053 487.
1054
1055 Obermuller, S., Calegari, F., King, A., Lindqvist, A., Lundquist, I., Salehi, A., Francolini,
1056 M., Rosa, P., Rorsman, P., Huttner, W.B., and Barg, S. (2010). Defective secretion of islet
1057 hormones in chromogranin-B deficient mice. PLoS One *5*, e8936.
1058
1059 Oda, Y., Okada, T., Yoshida, H., Kaufman, R.J., Nagata, K., and Mori, K. (2006). Derlin-
1060 2 and Derlin-3 are regulated by the mammalian unfolded protein response and are
1061 required for ER-associated degradation. J Cell Biol *172*, 383-393.
1062
1063 Paik, K.H., Jin, D.K., Lee, K.H., Armstrong, L., Lee, J.E., Oh, Y.J., Kim, S., Kwon, E.K.,
1064 and Choe, Y.H. (2007). Peptide YY, cholecystokinin, insulin and ghrelin response to meal
1065 did not change, but mean serum levels of insulin is reduced in children with Prader-Willi
1066 syndrome. J Korean Med Sci *22*, 436-441.
1067
1068 Parikh, R.A., Appleman, L.J., Bauman, J.E., Sankunny, M., Lewis, D.W., Vlad, A., and
1069 Gollin, S.M. (2014). Upregulation of the ATR-CHEK1 pathway in oral squamous cell
1070 carcinomas. Genes Chromosomes Cancer *53*, 25-37.
1071
1072 Park, S.K., Aslanian, A., McClatchy, D.B., Han, X., Shah, H., Singh, M., Rauniyar, N.,
1073 Moresco, J.J., Pinto, A.F., Diedrich, J.K., et al. (2014). Census 2: isobaric labeling data
1074 analysis. Bioinformatics *30*, 2208-2209.
1075
1076 Park, S.M., Kang, T.I., and So, J.S. (2021). Roles of XBP1s in transcriptional regulation
1077 of target genes. Biomedicines *9*, 791.
1078
1079 Plate, L., Cooley, C.B., Chen, J.J., Paxman, R.J., Gallagher, C.M., Madoux, F., Genereux,
1080 J.C., Dobbs, W., Garza, D., Spicer, T.P., et al. (2016). Small molecule proteostasis
1081 regulators that reprogram the ER to reduce extracellular protein aggregation. Elife *5*,
1082 e15550.
1083
1084 Preissler, S., and Ron, D. (2019). Early events in the endoplasmic reticulum unfolded
1085 protein response. Cold Spring Harb Perspect Biol *11*; a033894.
1086
1087 Proverbio, M.C., Mangano, E., Gessi, A., Bordoni, R., Spinelli, R., Asselta, R., Valin, P.S.,
1088 Di Candia, S., Zamproni, I., Diceglie, C., et al. (2013). Whole genome SNP genotyping
1089 and exome sequencing reveal novel genetic variants and putative causative genes in
1090 congenital hyperinsulinism. PLoS One *8*, e68740.
1091
1092 Rajpal, G., Schuiki, I., Liu, M., Volchuk, A., and Arvan, P. (2012). Action of protein disulfide
1093 isomerase on proinsulin exit from endoplasmic reticulum of pancreatic β-cells. J Biol
1094 Chem *287*, 43-47.
1095

1096 Ran, F.A., Hsu, P.D., Wright, J., Agarwala, V., Scott, D.A., and Zhang, F. (2013). Genome
1097 engineering using the CRISPR-Cas9 system. Nat Protoc *8*, 2281-2308.
1098
1099 Rapkins, R.W., Hore, T., Smithwick, M., Ager, E., Pask, A.J., Renfree, M.B., Kohn, M.,
1100 Hameister, H., Nicholls, R.D., Deakin, J.E., and Graves, J.A. (2006). Recent assembly of
1101 an imprinted domain from non-imprinted components. PLoS Genet *2*, e182.
1102
1103 Reinbothe, T.M., Alkayyali, S., Ahlqvist, E., Tuomi, T., Isomaa, B., Lyssenko, V., and
1104 Renstrom, E. (2013). The human L-type calcium channel Cav1.3 regulates insulin release
1105 and polymorphisms in CACNA1D associate with type 2 diabetes. Diabetologia *56*, 340-
1106 349.
1107
1108 Roder, P.V., Wu, B., Liu, Y., and Han, W. (2016). Pancreatic regulation of glucose
1109 homeostasis. Exp Mol Med *48*, e219.
1110
1111 Rorsman, P., and Braun, M. (2013). Regulation of insulin secretion in human pancreatic
1112 islets. Annu Rev Physiol *75*, 155-179.
1113
1114 Salpea, P., Cosentino, C., and Igoillo-Esteve, M. (2020). A review of mouse models of
1115 monogenic diabetes and ER stress signaling. Methods Mol Biol *2128*, 55-67.
1116
1117 Sandberg, A., Branca, R.M., Lehtio, J., and Forshed, J. (2014). Quantitative accuracy in
1118 mass spectrometry based proteomics of complex samples: the impact of labeling and
1119 precursor interference. J Proteomics *96*, 133-144.
1120
1121 Sandoval, D.A., and D'Alessio, D.A. (2015). Physiology of proglucagon peptides: role of
1122 glucagon and GLP-1 in health and disease. Physiol Rev *95*, 513-548.
1123
1124 Schuster, D.P., Osei, K., and Zipf, W.B. (1996). Characterization of alterations in glucose
1125 and insulin metabolism in Prader-Willi subjects. Metabolism *45*, 1514-1520.
1126
1127 Segerstolpe, A., Palasantza, A., Eliasson, P., Andersson, E.M., Andreasson, A.C., Sun,
1128 X., Picelli, S., Sabirsh, A., Clausen, M., Bjursell, M.K., et al. (2016). Single-cell
1129 transcriptome profiling of human pancreatic islets in health and type 2 diabetes. Cell
1130 Metab *24*, 593-607.
1131
1132 Sharma, R.B., Darko, C., and Alonso, L.C. (2020). Intersection of the ATF6 and XBP1 ER
1133 stress pathways in mouse islet cells. J Biol Chem *295*, 14164-14177.
1134
1135 Sharma, R.B., Landa-Galván, H.V., and Alonso, L.C. (2021). Living dangerously:
1136 protective and harmful ER stress responses in pancreatic β-cells. Diabetes *70*, 2431-
1137 2443.
1138
1139 Sharma, R.B., O'Donnell, A.C., Stamateris, R.E., Ha, B., McCloskey, K.M., Reynolds,
1140 P.R., Arvan, P., and Alonso, L.C. (2015). Insulin demand regulates β cell number via the
1141 unfolded protein response. J Clin Invest *125*, 3831-3846.
1142

1143 Shen, J., Chen, X., Hendershot, L., and Prywes, R. (2002). ER stress regulation of ATF6
1144 localization by dissociation of BiP/GRP78 binding and unmasking of Golgi localization
1145 signals. Dev Cell *3*, 99-111.
1146
1147 Skelin, M., Rupnik, M., and Cencic, A. (2010). Pancreatic beta cell lines and their
1148 applications in diabetes mellitus research. ALTEX *27*, 105-113.
1149
1150 Smith, T., Heger, A., and Sudbery, I. (2017). UMI-tools: modeling sequencing errors in
1151 Unique Molecular Identifiers to improve quantification accuracy. Genome Res *27*, 491-
1152 499.
1153
1154 Stefan, M., Ji, H., Simmons, R.A., Cummings, D.E., Ahima, R.S., Friedman, M.I., and
1155 Nicholls, R.D. (2005). Hormonal and metabolic defects in a Prader-Willi syndrome mouse
1156 model with neonatal failure to thrive. Endocrinology *146*, 4377-4385.
1157
1158 Stefan, M., Simmons, R.A., Bertera, S., Trucco, M., Esni, F., Drain, P., and Nicholls, R.D.
1159 (2011). Global deficits in development, function, and gene expression in the endocrine
1160 pancreas in a deletion mouse model of Prader-Willi syndrome. Am J Physiol Endocrinol
1161 Metab *300*, E909-922.
1162
1163 Sun, J., Cui, J., He, Q., Chen, Z., Arvan, P., and Liu, M. (2015). Proinsulin misfolding and
1164 endoplasmic reticulum stress during the development and progression of diabetes. Mol
1165 Aspects Med *42*, 105-118.
1166
1167 Sun, M., Kotler, J.L.M., Liu, S., and Street, T.O. (2019). The endoplasmic reticulum (ER)
1168 chaperones BiP and Grp94 selectively associate when BiP is in the ADP conformation. J
1169 Biol Chem *294*, 6387-6396.
1170
1171 Szczerbinska, I., Tessitore, A., Hansson, L.K., Agrawal, A., Ragel Lopez, A., Helenius,
1172 M., Malinowski, A.R., Gilboa, B., Ruby, M.A., Gupta, R., and Ammala, C. (2022). Large-
1173 scale functional genomics screen to identify modulators of human β-cell insulin secretion.
1174 Biomedicines *10*, 103.
1175
1176 Tabb, D.L., McDonald, W.H., and Yates, J.R., 3rd (2002). DTASelect and Contrast: tools
1177 for assembling and comparing protein identifications from shotgun proteomics. J
1178 Proteome Res *1*, 21-26.
1179
1180 Tauber, M., and Hoybye, C. (2021). Endocrine disorders in Prader-Willi syndrome: a
1181 model to understand and treat hypothalamic dysfunction. Lancet Diabetes Endocrinol *9*,
1182 235-246.
1183
1184 Teodoro, T., Odisho, T., Sidorova, E., and Volchuk, A. (2012). Pancreatic β-cells depend
1185 on basal expression of active ATF6α-p50 for cell survival even under nonstress
1186 conditions. Am J Physiol Cell Physiol *302*, C992-1003.
1187

1188 Teske, B.F., Wek, S.A., Bunpo, P., Cundiff, J.K., McClintick, J.N., Anthony, T.G., and
1189 Wek, R.C. (2011). The eIF2 kinase PERK and the integrated stress response facilitate
1190 activation of ATF6 during endoplasmic reticulum stress. Mol Biol Cell *22*, 4390-4405.
1191
1192 Tiwari, A., Schuiki, I., Zhang, L., Allister, E.M., Wheeler, M.B., and Volchuk, A. (2013).
1193 SDF2L1 interacts with the ER-associated degradation machinery and retards the
1194 degradation of mutant proinsulin in pancreatic β-cells. J Cell Sci *126*, 1962-1968.
1195
1196 Tomita, T., Greeley, G., Jr., Watt, L., Doull, V., and Chance, R. (1989). Protein meal-
1197 stimulated pancreatic polypeptide secretion in Prader-Willi syndrome of adults. Pancreas
1198 *4*, 395-400.
1199
1200 Tsuchiya, Y., Saito, M., Kadokura, H., Miyazaki, J.I., Tashiro, F., Imagawa, Y., Iwawaki,
1201 T., and Kohno, K. (2018). IRE1-XBP1 pathway regulates oxidative proinsulin folding in
1202 pancreatic β cells. J Cell Biol *217*, 1287-1301.
1203
1204 van Loon, N.M., Lindholm, D., and Zelcer, N. (2019). The E3 ubiquitin ligase inducible
1205 degrader of the LDL receptor/myosin light chain interacting protein in health and disease.
1206 Curr Opin Lipidol *30*, 192-197.
1207
1208 Watkins, S., Geng, X., Li, L., Papworth, G., Robbins, P.D., and Drain, P. (2002). Imaging
1209 secretory vesicles by fluorescent protein insertion in propeptide rather than mature
1210 secreted peptide. Traffic *3*, 461-471.
1211
1212 Wiseman, R.L., Mesgarzadeh, J.S., and Hendershot, L.M. (2022). Reshaping
1213 endoplasmic reticulum quality control through the unfolded protein response. Mol Cell *82*,
1214 1477-1491.
1215
1216 Wu, H., Yin, Q.F., Luo, Z., Yao, R.W., Zheng, C.C., Zhang, J., Xiang, J.F., Yang, L., and
1217 Chen, L.L. (2016). Unusual processing generates SPA lncRNAs that sequester multiple
1218 RNA binding proteins. Mol Cell *64*, 534-548.
1219
1220 Xin, Y., Dominguez Gutierrez, G., Okamoto, H., Kim, J., Lee, A.H., Adler, C., Ni, M.,
1221 Yancopoulos, G.D., Murphy, A.J., and Gromada, J. (2018). Pseudotime ordering of single
1222 human β-cells reveals states of insulin production and unfolded protein response.
1223 Diabetes *67*, 1783-1794.
1224
1225 Xu, T., Park, S.K., Venable, J.D., Wohlschlegel, J.A., Diedrich, J.K., Cociorva, D., Lu, B.,
1226 Liao, L., Hewel, J., Han, X., et al. (2015). ProLuCID: An improved SEQUEST-like
1227 algorithm with enhanced sensitivity and specificity. J Proteomics *129*, 16-24.
1228
1229 Ye, R., Jung, D.Y., Jun, J.Y., Li, J., Luo, S., Ko, H.J., Kim, J.K., and Lee, A.S. (2010).
1230 Grp78 heterozygosity promotes adaptive unfolded protein response and attenuates diet-
1231 induced obesity and insulin resistance. Diabetes *59*, 6-16.
1232
1233 Yin, Q.F., Yang, L., Zhang, Y., Xiang, J.F., Wu, Y.W., Carmichael, G.G., and Chen, L.L.
1234 (2012). Long noncoding RNAs with snoRNA ends. Mol Cell *48*, 219-230.

1235
1236 Yong, J., Johnson, J.D., Arvan, P., Han, J., and Kaufman, R.J. (2021). Therapeutic
1237 opportunities for pancreatic β-cell ER stress in diabetes mellitus. Nat Rev Endocrinol *17*,
1238 455-467.
1239
1240 Zhang, L., Lai, E., Teodoro, T., and Volchuk, A. (2009). GRP78, but not protein-disulfide
1241 isomerase, partially reverses hyperglycemia-induced inhibition of insulin synthesis and
1242 secretion in pancreatic β-cells. J Biol Chem *284*, 5289-5298.
1243
1244 Zhu, G., and Lee, A.S. (2015). Role of the unfolded protein response, GRP78 and GRP94
1245 in organ homeostasis. J Cell Physiol *230*, 1413-1420.
1246

FIGURES and FIGURE LEGENDS

Figure 1:

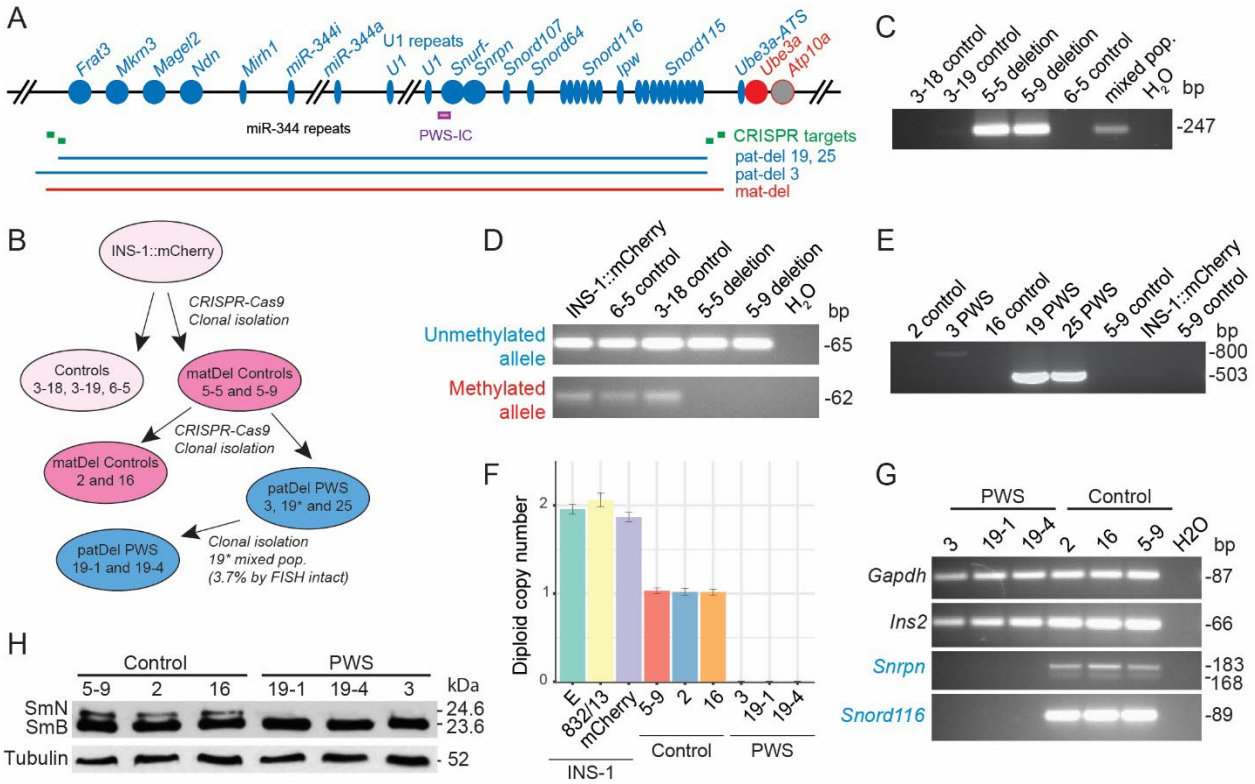

Figure 1. CRISPR/Cas9 genome editing to generate INS-1 lines with 3.16 Mb deletions of the silent (maternal) and active (paternal) PWS-imprinted domain. (A) Gene map of the rat PWS-imprinted domain and CRISPR/Cas9-targeted deletions. Symbols: circles, protein-coding genes; thin ovals, RNA genes; blue, (paternal; pat) and red (maternal; mat), imprinted genes; IC, imprinting control region (purple bar); green boxes, CRISPR gRNA target sites; blue and red horizontal bars, extent of deletions. Not all copies of tandemly repeated loci (*miR-344*; U1, *Snord116*, *Snord115*) are shown. **(B)** Schematic showing generation of genome edited, clonal INS-1 lines with 3.16 Mb deletions on the silent maternal allele only (5-9, 2, 16; dark pink) or homozygous deletion of both maternal and active paternal alleles (3, 19-1, 19-4, 25; blue). **(C)** First round deletion-PCR on genomic DNA identifies two INS-1 lines with deletions (5-9, 5-5). **(D)** DNA methylation analysis of bisulfite-modified genomic DNA at the PWS-IC establishes that lines 5-5 and 5-9 have deletions on the maternal allele. **(E)** Second round deletion-PCR identifies three INS-1 lines (3, 19, 25) with deletions on the paternal allele, with line 3 having an alternate proximal breakpoint. **(F)** Gene dosage of *Snord107* normalized to *Ube3a* as determined by ddPCR using genomic DNA from the INS-1 panel of cell lines (also see **Fig. S9**). **(G)** PWS-deletion lines (3, 19-1, 19-4) lack mRNA expression of the PWS-imprinted genes, *Snrpn* and *Snord116*, as detected by RT-PCR, whereas control lines (5-9, 2, 16) express PWS-imprinted genes. All cell lines express the control genes (*Gapdh*, *Ins2*). The full panel of PWS-imprinted genes is shown in **Fig. S10A,B**. **(H)** Use of whole cell extracts for a western blot shows that PWS-deletion lines (3, 19-1, 19-4) lack

1273 expression of the spliceosomal SmN polypeptide (24.6 kDa) encoded by *Snrpn*, but retain
1274 expression of the paralogous SmB polypeptide (23.6 kDa) encoded by the unlinked *Snrpb*
1275 gene. The control is α-Tubulin.

1276 **Figure 2:**

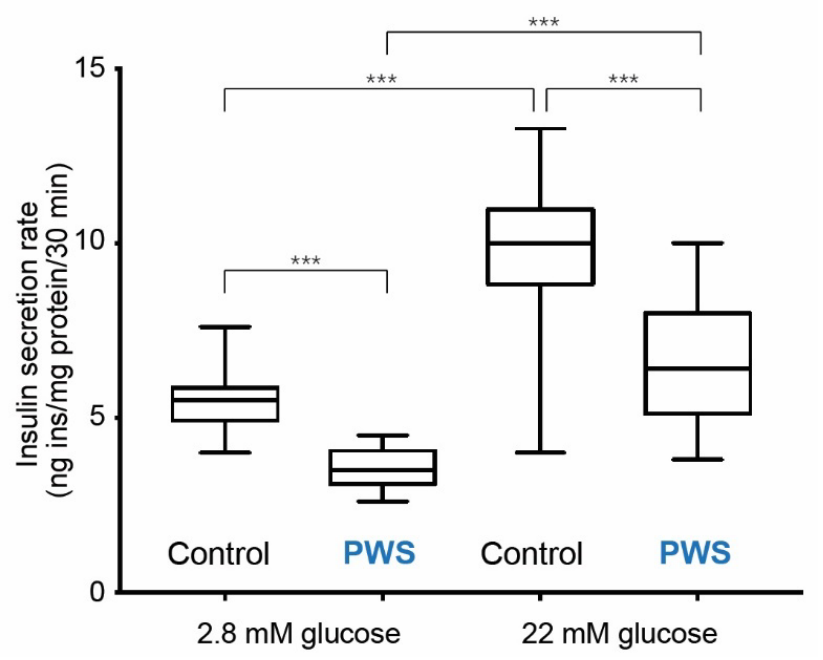

1277
1278
1279 **Figure 2. Deficient basal and GSIS in PWS-deletion INS-1 lines.** PWS INS-1 cell lines
1280 have insulin secretion deficits at both low (2.8 mM) and high (22 mM) glucose, based on
1281 the pooled insulin secretory rates for each of PWS (3, 19-1, 19-4) and control (5-9, 2, 16)
1282 groups (n=36 biological replicates per group, with n=12 per cell line). Although GSIS
1283 increased 1.75-fold for control and 1.85-fold for PWS, loss of the PWS genes decreased
1284 the secretory rate by 36% in basal 2.8 mM glucose conditions and by 32% in stimulatory
1285 22 mM glucose conditions. Statistical comparison by ANOVA with Tukey post hoc test
1286 (***, $P < 0.0001$).

1287 **Figure 3:**

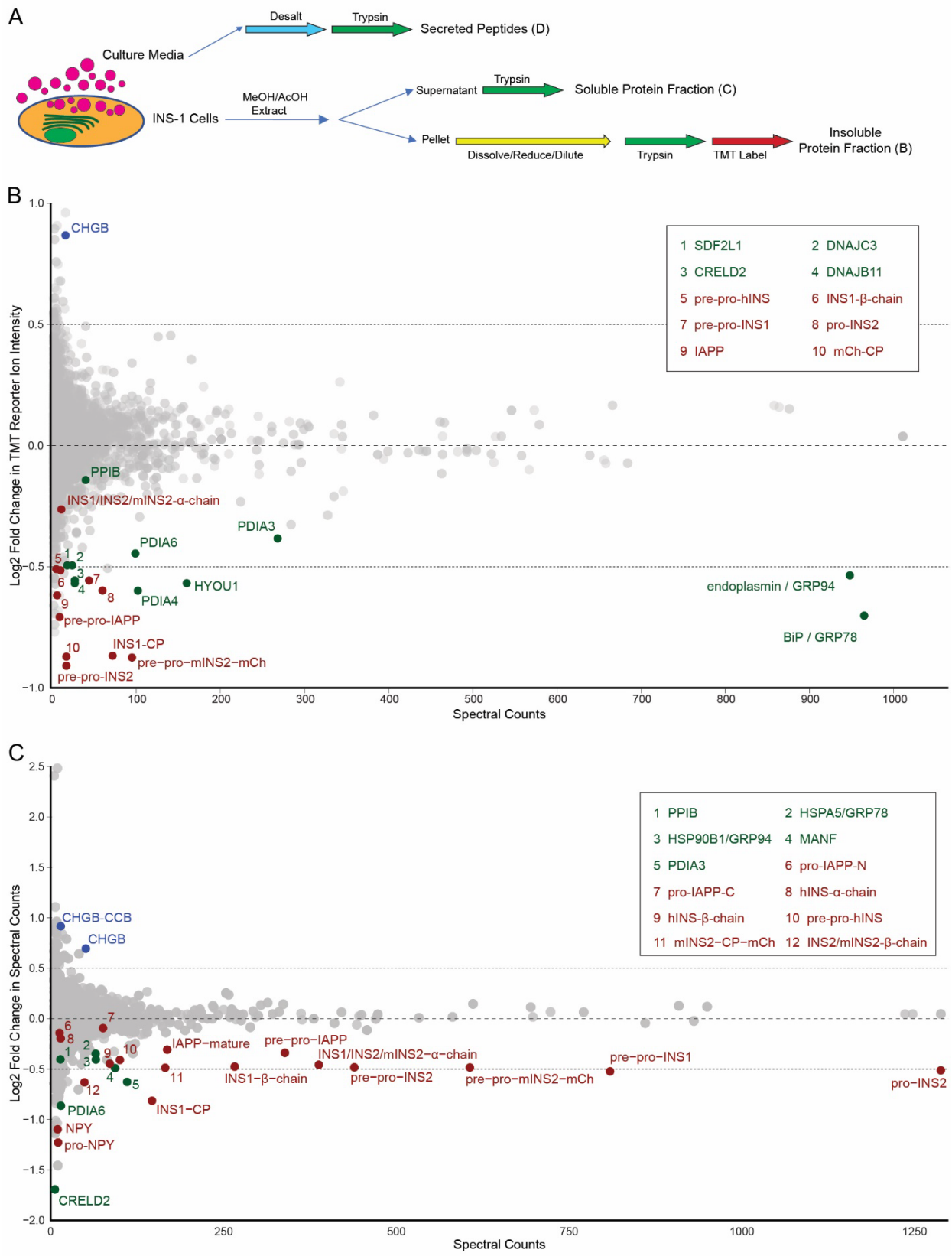

1288

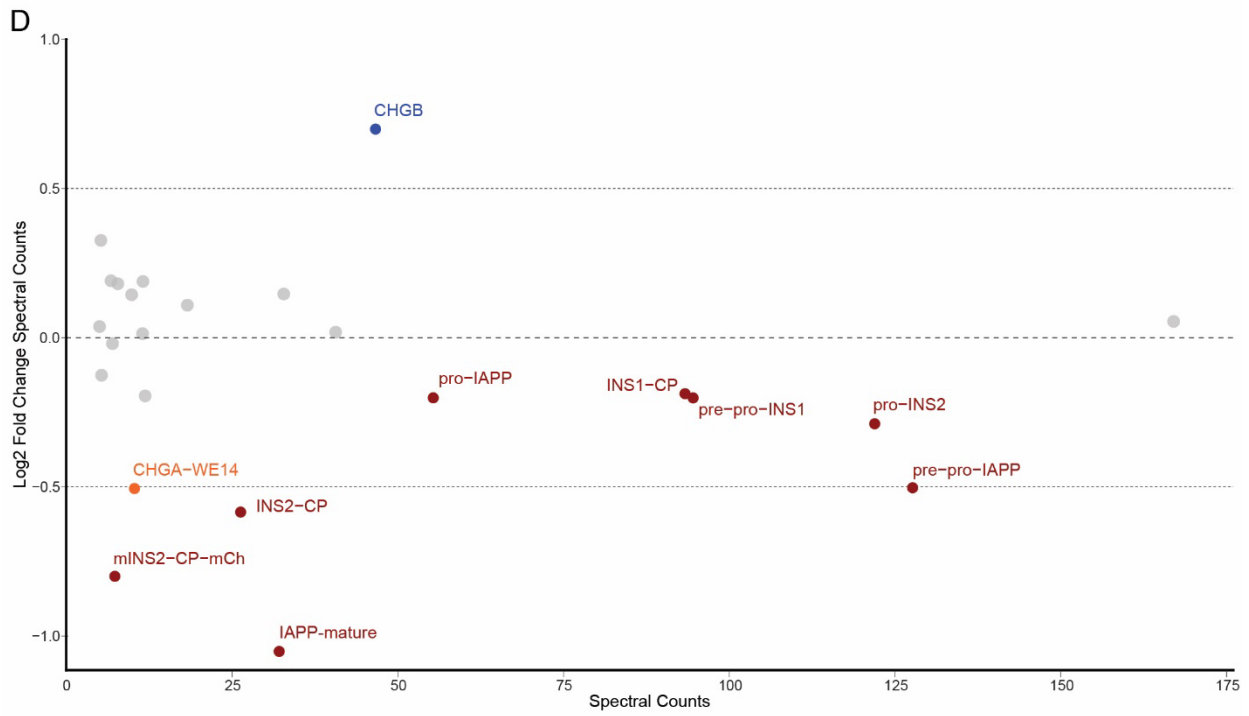

Figure 3. Proteome-wide alterations in PWS-deletion *vs.* control INS-1 lines identifies reductions in levels of ER chaperones and hormones. (A) Multiple fractions of PWS and control INS-1 cell cultures grown under GSIS conditions were assessed by mass spectrometry (MS). These included peptide hormones released from secretory granules (pink circles) into the media [see **Fig. 3D**] and cellular proteins methanol-acetic acid extracted into soluble proteins [see **Fig. 3C**], or an insoluble protein fraction assessed by quantitative Tandem Mass Tag (TMT) MS [see **Fig. 3B**]. **(B-D)** Relative protein detection of proteins in PWS of Log2 Fold Change (PWS/Control) of protein detection plotted against spectral counts indicating overall protein abundance. **(B)** Relative comparison of insoluble cellular proteins in PWS and control INS-1 β-cell lines detected by quantitative TMT MS. Protein levels of eleven ER chaperones (green) as well as secreted hormones (red) insulin [various processed forms of INS1, INS2, mouse (m) mINS2-mCherry (mCh), human (h) INS, and C-peptide (CP); mature INS is the 21 amino acid peptide identical between rat INS1, rat INS2 and mouse INS2] and amylin (full length and processed IAPP) were markedly reduced in PWS INS-1 cell lines. In contrast, chromogranin B (CHGB) levels are noticeably increased in PWS INS-1 cell lines (blue). The boxed Key indicates the identity of the 10 numbered peptide spots. **(C)** Comparison of soluble cellular peptides detected in PWS *vs.* control INS-1 lines, with reductions observed in PWS lines for highly expressed peptide hormones (red) including insulins [various processed forms of INS1, INS2, mINS2-mCh and CP], amylin (processed and unprocessed IAPP), and neuropeptide Y (processed and unprocessed NPY), as well as lower levels in the soluble fraction of the ER chaperones (green). Additionally, two isoforms of chromogranin B (full-length CHGB and the CCB C-terminal fragment of chromogranin B) are increased in PWS INS-1 cell lines (blue). The boxed Key indicates the identity of the 12 numbered peptide spots. **(D)** Comparison of secreted peptides highlighting reduced levels for PWS relative to control INS-1 lines for numerous secreted hormones (red) including insulins [various processed forms of INS1, INS2, mINS2-mCh

1317 and CP] and amylin (processed and unprocessed IAPP), as well as reduced secreted
1318 levels from PWS INS-1 lines of the CHGA-derived WE14 peptide (orange), while secreted
1319 levels of CHGB (blue) were increased in PWS INS-1 cell lines.

Figure 4:

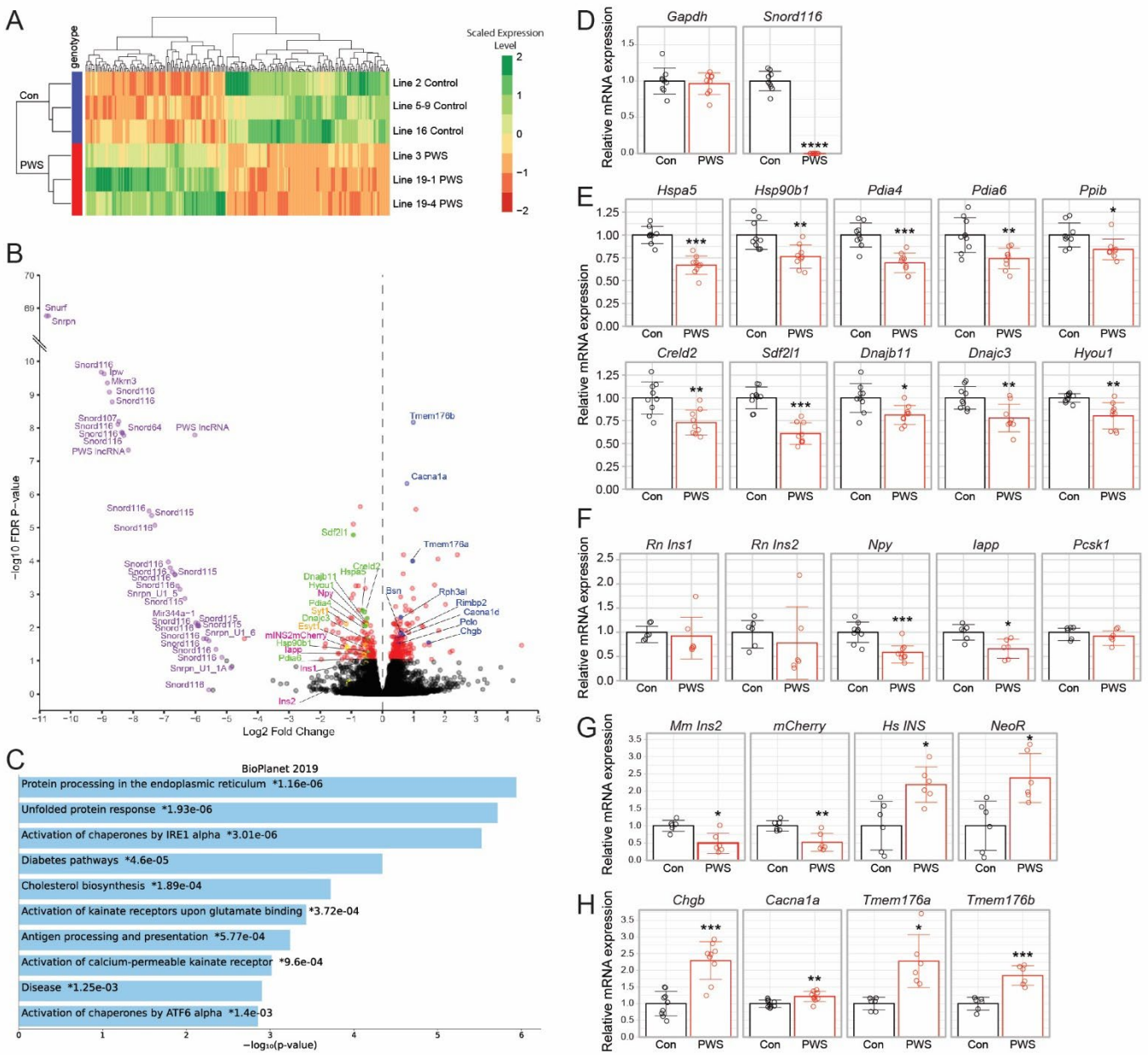

Figure 4. Genome-wide transcriptome alterations in PWS-deletion *vs.* control INS-1 lines identifies significant differentially expressed genes (DEGs) including those encoding ER chaperones and hormones. (A) Heatmap clustergram of 228 DEGs demonstrates tight clustering of PWS *vs.* control groups (*Padj* < 0.05). Scale: green (enriched) to red (depleted). RNA-seq was performed for 3 PWS (3, 19-1, 19-4) *vs.* 3 control (5-9, 2, 16) INS-1 cell lines. **(B)** Volcano plot showing statistical significance (-log10 FDR *P*-value) *vs.* magnitude of change (Log2 Fold Change) for all expressed genes. Colored data points indicate PWS-imprinted genes (purple), ER chaperones (green), secreted proteins (pink), synaptotagmins involved in insulin secretion (yellow), proteins involved in neuronal active zone/exocytosis and vesicle acidification (blue), and all other significant genes (red, without labels). **(C)** Gene set enrichment analysis

1333 identifies key biological pathways involved in protein processing and the unfolded stress
1334 response in the ER. **(D-H)** Relative gene expression of control (Con, black; 5-9, 2, 16) *vs.*
1335 PWS (red; 3, 19-1, 19-4) determined by RT-ddPCR normalized to *Gpi* levels and to the
1336 average expression in control INS-1 lines, including for **(D)** *Gapdh* and *Snord116* (PWS)
1337 control genes, **(E)** ten downregulated DEGs encoding ER chaperones, **(F)** endogenous
1338 *Rattus norvegicus* (Rn) genes encoding β-cell hormones and secretory proteins, **(G)**
1339 exogenous insulin transgenes in the INS-1 lines (*Mm*, *Mus musculus*; *Hs*, *Homo sapiens*)
1340 as well as mCherry and neomycin resistance (*Neo*R) marker proteins, and **(H)**
1341 upregulated DEGs involved in the secretory pathway. Statistical comparison by Welch's
1342 t-test: *, $P < 0.05$; **, $P < 0.005$; ***, $P < 0.0005$; ****, $P < 0.00005$.

Figure 5:

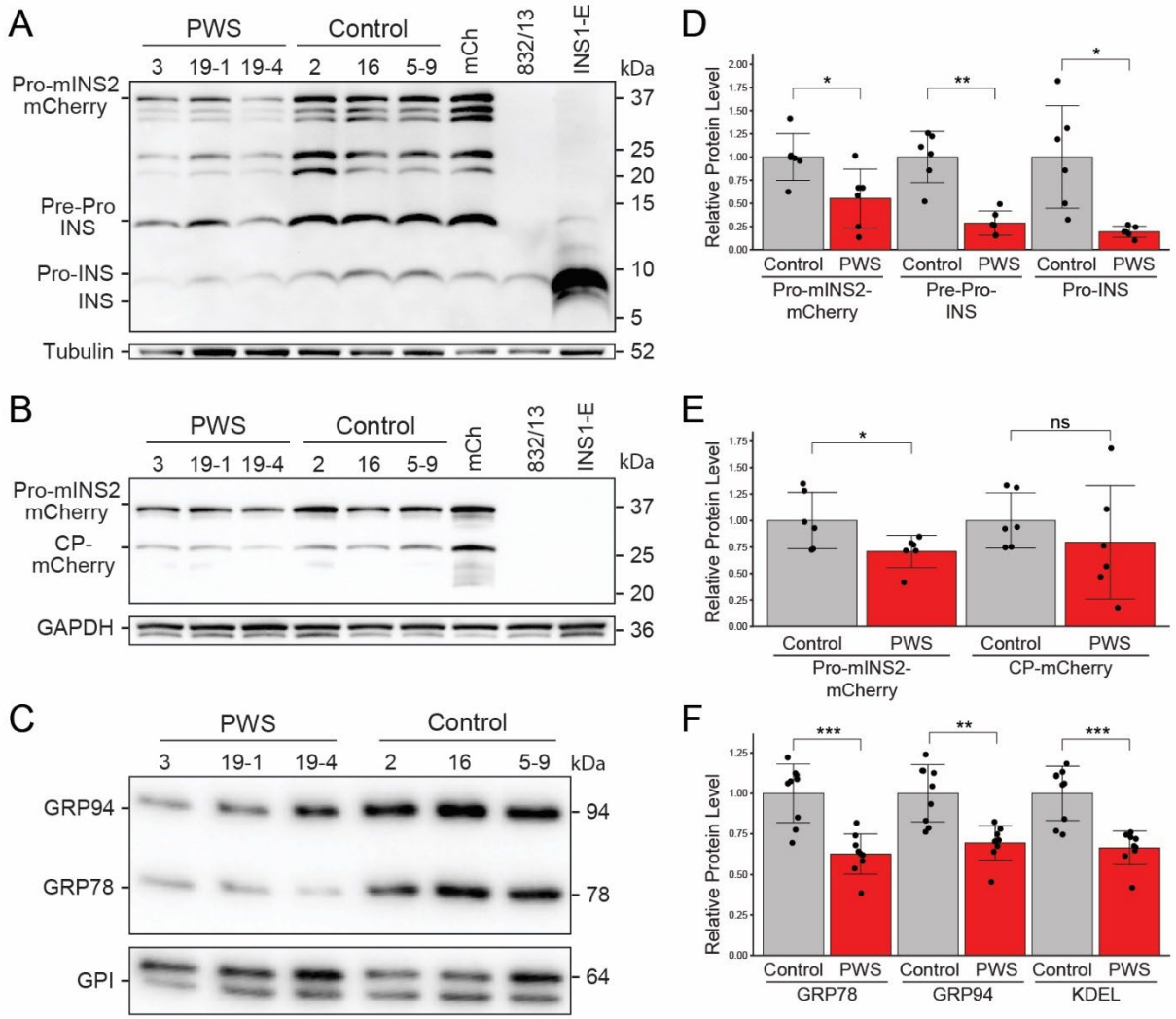

Figure 5. Reductions in insulins and ER chaperone levels in PWS-deletion *vs.* control INS-1 lines. (A-C) Western blots of whole cell lysates from PWS (3, 19-1, 19-4) and control (5-9, 2, 16) INS-1 β-cell lines grown under control (DMSO) conditions for 5 h were assessed using a panel of antibodies. **(A)** Anti-insulin, detecting all cellular forms of insulin (Pre-Pro-, Pro-, and fully processed rat INS) as well as mouse proinsulin2 (Pro-mINS2)-mCherry. **(B)** Anti-mCherry, detecting mouse proinsulin2 (Pro-mINS2)-mCherry and C-peptide (CP)-mCherry. **(C)** Anti-KDEL, detecting the two major ER chaperones GRP94 (endoplasmin; HSP90B1) and GRP78 (BiP; HSPA5). Anti-α-Tubulin, anti-GAPDH, and anti-GPI were used as controls for protein loading levels in **(A)**, **(B)**, and **(C)**, respectively. For **(A)** and **(B)**, control cell lines included INS-1::mCherry (mCh), INS-1(832/13) parental, and INS1-E. **(D)** Quantitation of Pro-mINS2-mCherry, Pre-Pro-INS and Pro-INS detected with anti-insulin in the PWS and control INS-1 lines (n=6 each genotype). **(E)** Quantitation of Pro-mINS2-mCherry and CP-mCherry detected with anti-mCherry in the PWS and control INS-1 lines (n=6 each). **(F)** Quantitation of GRP78, GRP94, and total KDEL detected with anti-KDEL in the PWS and control INS-1 lines (n=9

1361 each). For **(D-F)**, statistical comparison by Welch's t-test: *, $P < 0.05$; **, $P < 0.005$; ***, P
1362 < 0.0005; ns, not significant.

Figure 6:

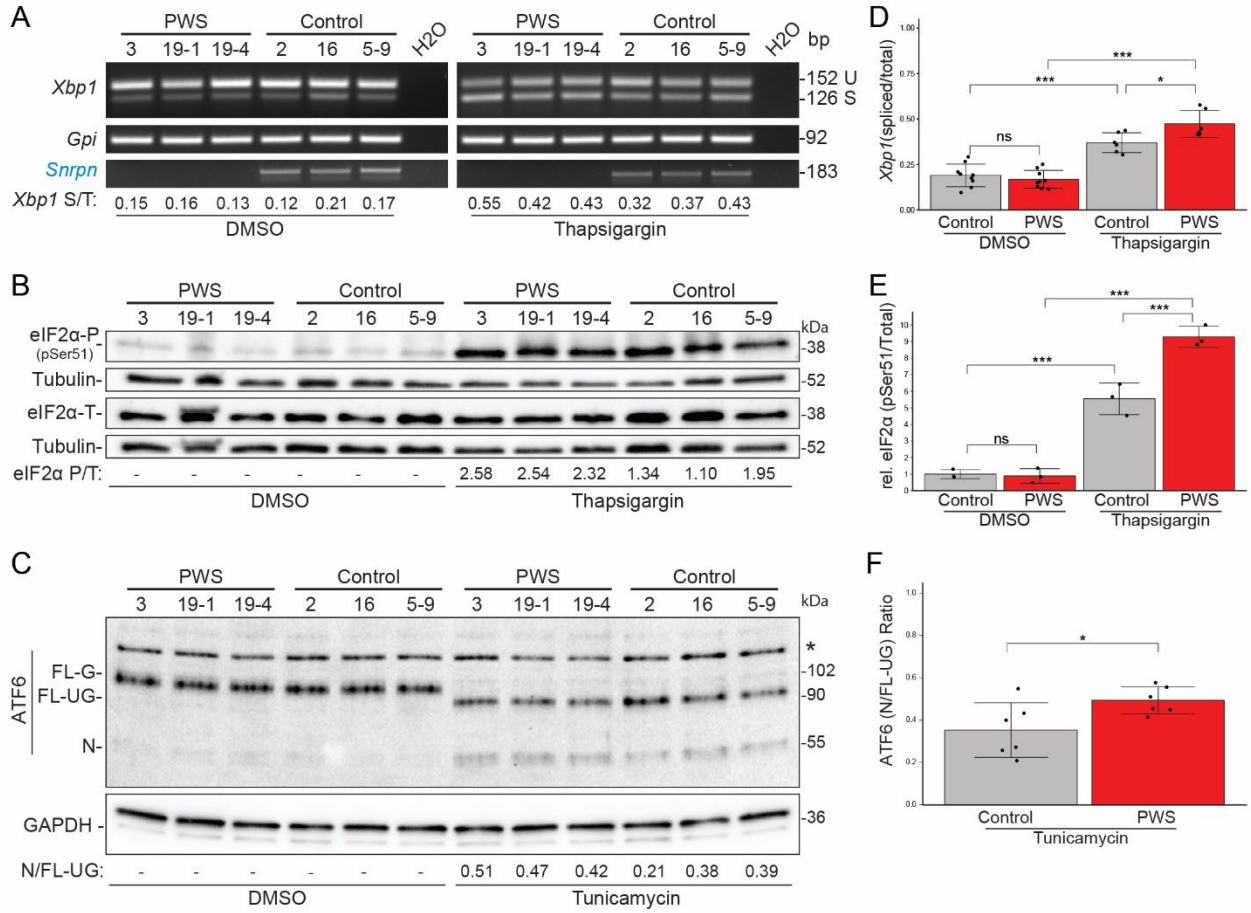

Figure 6. More sensitive activation of all three ER stress master regulatory pathways in PWS-deletion *vs.* control INS-1 β-cell lines. (A) For the IRE1α pathway, we assessed its mRNA processing of *Xbp1* from unspliced (U) to spliced (S), with control gene *Gpi* and PWS-*Snord116* also assayed by RT-PCR, using RNA from PWS (3, 19-1, 19-4) and control (5-9, 2, 16) INS-1 cell lines treated with DMSO or 0.1 μM thapsigargin for 3 h. At bottom, the *Xbp1* S/T (spliced/total) ratios for each cell line are shown, under both control (DMSO) and ER stress (thapsigargin) conditions. **(B)** The PERK pathway was assessed by comparison of total eIF2α to PERK phosphorylated eIF2α-P (pSer51), using whole cell lysates from PWS and control INS-1 cell lines treated with DMSO or 0.1 μM thapsigargin for 5 h. Anti-αTUB was used as a control for protein-loading levels. At bottom, the eIF2α P/T (phosphorylated/total) ratios for each cell line are shown under the ER stress (thapsigargin) condition. **(C)** For the ATF6 pathway, we used whole cell lysates from PWS and control INS-1 cell lines treated with DMSO or 10 μg/ml tunicamycin for 5 h. Under control DMSO conditions, full-length (FL) and glycosylated (G) ATF6 of ~ 100-kD is ER-localized. tunicamycin inhibits biosynthesis of N-linked glycans, resulting in unglycosylated (UG) ATF6-FL of 90-kD in the ER, with proteolytic processing in the Golgi to produce nuclear (N) ATF6-N of ~ 55-kD. *, non-specific band detected by the anti-ATF6 antibody. Anti-GAPDH was used as a control for protein-loading levels. At bottom, the ATF6 N/FL-UG (nuclear/FL-unglycosylated) ratios for each cell line are shown under the

1386 ER stress (tunicamycin) condition. **(D)** Quantitation of the ratio of spliced/total (S/T) *Xbp1*
1387 mRNA in the PWS and control INS-1 lines under control (DMSO; n=9 each genotype)
1388 and thapsigargin (3 h; n=6 each) conditions. PWS β-cells are more sensitive to
1389 thapsigargin-induced ER stress with earlier and more robust activation of *Xbp1* mRNA
1390 "splicing" than control cell lines. **(E)** Quantitation of the relative (rel.) level of
1391 phosphorylated (pSer51) to total eIF2α in the PWS and control INS-1 lines (n=3 each)
1392 under control (DMSO) and thapsigargin conditions. PWS cells are more sensitive to
1393 thapsigargin-induced ER stress with more robust activation of eIF2α phosphorylation. **(F)**
1394 Quantitation of the ratio of nuclear/FL-unglycosylated (N/UG) for ATF6 in the PWS and
1395 control INS-1 lines under ER stress (tunicamycin) conditions (n=6 each, from two
1396 biological replicates). PWS cells are more sensitive to tunicamycin-induced ER stress
1397 with more robust activation of ATF6-N. For **(D-E)**, statistical comparison by ANOVA and
1398 for **(F)** by Welch's t-test with Tukey's HSD post-hoc: *, $P < 0.05$; **, $P < 0.005$; ***, $P <$
1399 0.0005; ns, not significant.